



An attempt at
estimating Paris area
CO₂ emissions

F. M. Bréon et al.

This discussion paper is/has been under review for the journal Atmospheric Chemistry and Physics (ACP). Please refer to the corresponding final paper in ACP if available.

An attempt at estimating Paris area CO₂ emissions from atmospheric concentration measurements

F. M. Bréon¹, G. Broquet¹, V. Puygrenier¹, F. Chevallier¹, I. Xueref-Rémy¹, M. Ramonet¹, E. Dieudonné¹, M. Lopez¹, M. Schmidt¹, O. Perrussel², and P. Ciais¹

¹Laboratoire des Sciences du Climat et de l'Environnement, UMR CEA-CNRS-UVSQ, Gif sur Yvette, France

²AirParif, 7 rue Crillon, Paris, France

Received: 22 January 2014 – Accepted: 3 April 2014 – Published: 10 April 2014

Correspondence to: F. M. Bréon (breon@lsce.ipsl.fr)

Published by Copernicus Publications on behalf of the European Geosciences Union.

Title Page

Abstract

Introduction

Conclusions

References

Tables

Figures



Back

Close

Full Screen / Esc

Printer-friendly Version

Interactive Discussion



Abstract

Atmospheric concentration measurements are used to adjust the daily to monthly budget of CO₂ emissions from the AirParif inventory of the Paris agglomeration. We use 5 atmospheric monitoring sites including one at the top of the Eiffel tower. The atmospheric inversion is based on a Bayesian approach, and relies on an atmospheric transport model with a spatial resolution of 2 km with boundary conditions from a global coarse grid transport model. The inversion tool adjusts the CO₂ fluxes (anthropogenic and biogenic) with a temporal resolution of 6 h, assuming temporal correlation of emissions uncertainties within the daily cycle and from day to day, while keeping the a priori spatial distribution from the emission inventory.

The inversion significantly improves the agreement between measured and modelled concentrations. However, the amplitude of the atmospheric transport errors is often large compared to the CO₂ gradients between the sites that are used to estimate the fluxes, in particular for the Eiffel tower station. In addition, we sometime observe large model-measurement differences upwind from the Paris agglomeration, which confirms the large and poorly constrained contribution from distant sources and sinks included in the prescribed CO₂ boundary conditions

These results suggest that (i) the Eiffel measurements at 300 m above ground cannot be used with the current system and (ii) the inversion shall rely on the measured upwind-downwind gradients rather than the raw mole fraction measurements. With such setup, realistic emissions are retrieved for two 30 day periods. Similar inversions over longer periods are necessary for a proper evaluation of the results.

1 Introduction

Although the total CO₂ emissions of developed countries may be well constrained from the total consumption of fossil fuel, its spatial and temporal distribution are not known with the same level of accuracy. Due to the high population density associated with

ACPD

14, 9647–9703, 2014

An attempt at estimating Paris area CO₂ emissions

F. M. Bréon et al.

Title Page

Abstract

Introduction

Conclusions

References

Tables

Figures

◀

▶

◀

▶

Back

Close

Full Screen / Esc

Printer-friendly Version

Interactive Discussion



An attempt at estimating Paris area CO₂ emissions

F. M. Bréon et al.

Title Page

Abstract

Introduction

Conclusions

References

Tables

Figures

◀

▶

◀

▶

Back

Close

Full Screen / Esc

Printer-friendly Version

Interactive Discussion

ground transportation, residence and industry, anthropogenic CO₂ emissions are large within cities (Pataki et al., 2006). The emitted CO₂ is transported in the atmosphere and results in elevated CO₂ concentration domes or plumes above and downwind of cities. The mole fraction signal above the background, as can be measured at a given location, is proportional to the net CO₂ flux of the local source that influences this location, i.e. to the sum of fossil fuel emissions, net ecosystem exchange (NEE) by plants and soils, and other emissions (decaying products that emit CO₂ to the atmosphere, human and animal respiration. . .). There is therefore a potential to estimate the net CO₂ flux of a city from a few atmospheric concentration measurements located within or in the vicinity of the city (McKain et al., 2012). Over a very dense urban area, the net CO₂ flux is dominated by fossil fuel emissions, but over less dense urban structures, NEE becomes significant and can partly offset fossil CO₂ emissions during the growing season (Nordbo et al., 2012).

Net CO₂ flux estimates, including fossil fuel emissions, constrained by independent atmospheric measurements could come in complement to, or for the assessment of current estimates that rely on bottom-up inventories based upon various activity data (Gurney et al., 2012). In inventories, CO₂ emission is calculated as a combination of geo-referenced activity proxies (e.g. traffic data or number and type of buildings that relate to residential emissions) multiplied by emission factors, accounting for the disaggregation of national budgets. The accuracy of the bottom-up estimates is seldom assessed and mostly relies on the difference between various estimates or expert knowledge on emission factors. An independent or complementary top-down method of evaluation based upon atmospheric measurements would be welcome, if its accuracy can be demonstrated to be equivalent for verification or significantly better. Atmospheric concentration measurements may also be used to improve (i.e. correct) the existing inventories. The estimate of surface fluxes from atmospheric concentration measurements requires mesoscale networks of CO₂ stations, and an accurate modelling of the atmospheric transport processes.

An attempt at estimating Paris area CO₂ emissions

F. M. Bréon et al.

Title Page

Abstract

Introduction

Conclusions

References

Tables

Figures

◀

▶

◀

▶

Back

Close

Full Screen / Esc

Printer-friendly Version

Interactive Discussion



The technique of estimating surface CO₂ fluxes from atmospheric composition measurements and potentially prior information- is relatively mature. It has been used for many years to estimate the biogenic fluxes at the global (Gurney et al., 2002; Chevallier et al., 2010), continental (Broquet et al., 2013; Peylin et al., 2005) and regional (Lauvaux et al., 2009, 2012) scales. However, because of uncertainties in the atmospheric transport, insufficient measurement sampling, and inconsistencies between the mathematical framework hypothesis of most inversions (no biases, Gaussian distribution of errors, error correlations. . .) and the reality, the results are often unreliable, as shown through a comparison of global and continental-scale biogenic flux estimates by several groups (Peylin et al., 2013).

Although the mathematical and modelling tools are similar, estimating the net CO₂ flux of a city faces specific challenges. One difficulty lies in the spatial heterogeneity of the source. This heterogeneity and the possibility of having very high emission fluxes locally (e.g. a power plant) make the concentration plume highly variable. Relating mole fractions to fluxes requires an accurate atmospheric transport model at fine scale. Another difficulty, shared with biogenic fluxes, lays in the temporal variability of the emissions, which have a strong daily cycle but also day-to-day variability resulting from, for instance, temperature changes (heating) or activity variability (traffic).

This challenge has been addressed recently by several research projects, e.g. IN-FLUX (sites.psu.edu/influx/), over the Indianapolis city or Megacities (http://megacities.jpl.nasa.gov; Duren and Miller, 2012) over Los Angeles, which have set-up a number (5 to 10) of surface, tower and airborne measurements of the atmospheric mole fractions. The analyses of an ongoing urban CO₂ measurement project at Salt Lake City showed the need for accurate atmospheric transport simulation at high-resolution with some urban scheme (Nehrkorn et al., 2013). The results indicated that monthly emission changes of 15 % could be detected at the 95 % confidence level with the current monitoring system (McKain et al., 2012). The CO₂-MegaParis project has a similar objective for the Paris area. This is a potentially favourable area as the city is very dense and the emissions intense over a limited area, with a fairly flat topography in the surround-

An attempt at estimating Paris area CO₂ emissions

F. M. Bréon et al.

[Title Page](#)[Abstract](#)[Introduction](#)[Conclusions](#)[References](#)[Tables](#)[Figures](#)[Back](#)[Close](#)[Full Screen / Esc](#)[Printer-friendly Version](#)[Interactive Discussion](#)

ings and rural areas around the city, which makes the atmospheric transport modelling and identification of the emission plume easier. A pilot campaign early 2010 was conducted in the framework of the MEGAPOLI project. Measurements of CO₂ mole fractions and its isotopes have been used to estimate the relative contribution of fossil and biogenic emissions in the concentration gradients (Lopez et al., 2013). The main campaign started in August 2010 with the installation of 3 CO₂ and CO monitoring stations within the city and its surrounding that provided near-continuous measurements until July 2011. These three stations complement two stations of the ICOS France network located in the Paris region outside the city that have been operational for several years. Lac et al. (2013) made a first analysis of the measurements and a comparison against atmospheric modelling using the Meso-NH mesoscale transport model, combined with an urban-meteorological model, for a period of 5 days in March 2011. They demonstrated the ability of the modelling framework to reproduce several features of the mole fraction daily cycle and of the mixing layer height.

Large efforts have been made by AirParif, the air quality agency for the Paris area, to generate an inventory of the Paris area emissions, for various pollutants and for CO₂ as well. The AirParif emission inventory, detailed in Sect. 2.2, provides an hourly description of the CO₂ emissions at ≈ 1 km resolution for representative weekdays and months. We shall use this inventory as a prior and use the atmospheric concentration measurements from 5 sites to assess whether the model results are compatible with the observations and to attempt an adjustment of the fluxes as suggested by the model-measurement mismatches. Clearly, with only 5 stations in the vicinity of the city, there is insufficient information to constrain the spatial distribution of the emissions. We therefore only attempt a rescaling of the emissions, relying on the spatial distribution provided by the Airparif inventory. For the inversion, NEE and fossil fuel emissions are optimized separately without making other fluxes (such as human respiration) explicit. We focus on two 30 day periods in the fall of 2010. This choice is driven by the expectation of rather small biogenic fluxes during this time period, which makes easier the interpretation of the measurements in terms of anthropogenic fluxes. Our objec-

tive is to assess whether a reliable estimate of the emissions can be derived from the combination of atmospheric measurements, available inventories and information on the atmospheric transport. A forthcoming paper will apply the methodology to a full year of observations and analyse the result for the spring and summer periods, when CO₂ uptake by NEE can partially offset fossil fuel emissions (Pataki et al., 2007). In the following, Sect. 2 analyses the time series of measured and modelled CO₂ mole fractions; Sect. 3 describes the methodology to correct the inventory based on the measurement-model mismatches. The results are shown in Sects. 4 and 5, using two different inversion setups. Section 6 discusses the results and concludes.

2 Measurements and direct simulations

2.1 CO₂ concentration measurements

In this paper, we use CO₂ mole fraction measurements that have been acquired in the framework of the CO₂-Megaparis and ICOS-France projects. Three stations have been equipped with high precision CO₂/CO analysers (Picarro G1302) specifically for the project objectives. One is located in the heart of Paris, at the summit of the Eiffel tower (300 m above the surface). Two are located in the North (semi-urban) and North-East (semi-rural) of the Paris area. These stations are complemented by two others that were operational before the start of the project. One is located in the South West, about 20 km from the centre of Paris (semi-rural), while the other is a tall tower located further south by about 100 km (rural). Both are using gas chromatograph analyzers (Agilent HP6890). The location of the stations are given in Table 1 and shown in Fig. 1. These 5 stations are very roughly located along a NE–SW direction, which define favourable wind directions for the monitoring of the emissions from this observation network, with a station at the edge of the urban area in both directions. All 5 stations are equipped with continuous monitoring instruments. The measurements are quality-controlled and binned at a temporal resolution of 1 h. They have been regularly calibrated against the

An attempt at estimating Paris area CO₂ emissions

F. M. Bréon et al.

Title Page

Abstract

Introduction

Conclusions

References

Tables

Figures



Back

Close

Full Screen / Esc

Printer-friendly Version

Interactive Discussion



An attempt at estimating Paris area CO₂ emissions

F. M. Bréon et al.

Title Page

Abstract

Introduction

Conclusions

References

Tables

Figures



Back

Close

Full Screen / Esc

Printer-friendly Version

Interactive Discussion



WMO mole fraction scale (Zhao and Tans, 2006) and the measurement repeatability is then expected to be better than 0.3 ppm. Two monitoring sites are located high above the surface (180 m and 300 m for the rural tall tower in the South and the top of the Eiffel tower, respectively) but the other ones are only a few meters above the ground. During the night and morning, the atmosphere is often very stable so that surface emissions accumulate within the lowest atmospheric layers (a few meters to tens of meters). The atmospheric mole fraction is then mostly sensitive to local fluxes and local atmospheric stability – an atmospheric state variable which is difficult to model – and there is a large uncertainty on the link between the emissions and the atmospheric mole fraction. As a consequence, we focus on the concentration measurements acquired during the afternoon only, from noon to 4 p.m., when the mixing layer is usually well developed. Note that, due to the longitude of Paris, UT time and solar times are very similar.

2.2 AirParif inventory

The AirParif air quality agency (<http://www.airparif.asso.fr/en/index/index>) has developed an inventory of emissions (for greenhouse gases such as CO₂ but also air pollutants) at 1 km spatial resolution and hourly time step for the Île-de-France region. Île-de-France is the administrative region spreading typically within 60 km around the Paris city, the boundaries of which are shown in Fig. 1. The emissions are quantified by sectors. The improvement of methodologies and emission factors lead to frequent updates of the emission estimates.

Nearly eighty different sources types are included in the inventory with three main classes: point sources, linear and diffuse sources. Point sources correspond to large industries, power plants, and trash burning; linear sources are related to transportation, while diffuse sources are mostly associated to the residential sector and commercial activities. The road traffic emission estimates uses a traffic model and vehicles counting devices that report the number of vehicles and their average speed over almost 40 000 km portions of roadways. Large industries are requested to report their CO₂ emissions and these are used in the inventory. For smaller industrial sources that are

the inventory includes injection heights that have been used in the source term of the simulations.

2.3 Biogenic fluxes

The Net Ecosystem Exchange (NEE) flux maps used here are provided by the land surface component of the ECMWF forecasting system, C-TESSSEL (Boussetta et al., 2013). They are extracted from the ECMWF operational archives at the highest available resolution: 15 km and 3 h. These data are interpolated in space (2 to 10 km) and time (1 h) to be consistent with our model grid and temporal resolution.

Figure 4 shows the mean daily cycle of NEE for the Île-de-France area and for the 12 calendar months. There are large diurnal and seasonal NEE cycles. The flux is positive (emission) during the night and negative (uptake) during the day, even during the winter months, given the rather mild winter temperature prevailing over the Paris area. Nevertheless, the amplitude of the daily cycle of NEE is much larger in summer than it is in winter. The NEE values are of similar magnitude than the anthropogenic emissions with a strong anti-correlation on the daily cycle (negative NEE vs. large anthropogenic emissions during daytime; positive NEE and smaller anthropogenic emissions during the night). During the winter, NEE is relatively small and the anthropogenic emissions clearly dominate, but daytime NEE still offsets on average $\sim 20\%$ of the emissions, according to the C-TESSSEL model simulations. During spring and summer, however, the daytime NEE uptake is larger in absolute value than the anthropogenic emissions as shown through a comparison of Figs. 3 and 4.

The present paper focuses on two 30 day periods that start on 21 October and 27 November 2010. During these periods, the monthly mean hourly NEE fluxes are less than 3 kt CO_2 per hour over the Île-de-France area. NEE is then small, but not negligible, compared to anthropogenic emissions during the chosen inversion period. The direct simulations and the atmospheric inversion thus account explicitly for the biogenic fluxes.

An attempt at estimating Paris area CO₂ emissions

F. M. Bréon et al.

Title Page

Abstract

Introduction

Conclusions

References

Tables

Figures

◀

▶

◀

▶

Back

Close

Full Screen / Esc

Printer-friendly Version

Interactive Discussion



2.4 Atmospheric transport modelling

Atmospheric transport modelling provides the link between the surface fluxes and the mole fractions. Here, we use the Chimere transport model (Menut et al., 2013) with a resolution of 2 km around the Paris city, and 10 km for the surrounding of the modelling domain (see Fig. 1). There are 118 × 118 pixels in the modelling grid, and it covers an area of approximately 500 × 500 km². There are 19 layers on the vertical, from the surface to 500 hPa. The model is driven by ECMWF-analysed meteorology at 15 km resolution. There is no urban scheme in the atmospheric modelling that is used here.

The model transports the mole fractions that are determined by the surface fluxes and the boundary conditions. The prior surface fluxes (i.e. the fluxes before the atmospheric inversion) are the sum of

- Anthropogenic fossil fuel CO₂ emission within the Île-de-France region, from the AirParif inventory, as described in Sect. 2.2 and shown in Fig. 2.
- Anthropogenic fossil fuel CO₂ emissions outside the Île-de-France region, according to the Edgar database (Edgar, 2011) available at 10 km resolution. These are only annual fluxes, and there is no diurnal or seasonal cycle.
- Biogenic fluxes from the C-TESSEL land surface model, as described in Sect. 2.3

The CO₂ boundary conditions prescribed at the edges of the Chimere domain, and transported inside the domain by Chimere, are obtained from a global simulation (V10.2) from the LMDz transport model with a resolution of 3.75° (longitude) × 2.5° (latitude) (Chevallier et al., 2010). In this simulation, the surface fluxes have been optimized to fit the mole fractions measured at a number of stations distributed over the world, given their assigned uncertainty and given some prior information of the surface fluxes. Nevertheless, given the relatively coarse spatial resolution of the LMDz model, CO₂ boundary conditions are temporally and spatially very smooth and will be shown to have little impact on the spatial gradients simulated within the domain area.

An attempt at estimating Paris area CO₂ emissions

F. M. Bréon et al.

Title Page

Abstract

Introduction

Conclusions

References

Tables

Figures

◀

▶

◀

▶

Back

Close

Full Screen / Esc

Printer-friendly Version

Interactive Discussion



2.5 Direct CO₂ transport simulations

Figures 5 and A1 show the time series of the CO₂ mole fractions together with an indication of the modelled wind speed and direction to help the interpretation of the results. These time series are derived from observations and direct atmospheric modelling as described in Sect. 2.4. The blue line is the LMDZ modelled mole fraction that is transported from the domain boundaries, with additional contribution from anthropogenic emissions outside the Île-de-France region (Edgar fluxes). The green line shows the modelled mole fraction that includes the same contributions, plus the biogenic fluxes within the modelling domain and the anthropogenic emissions within the Île-de-France region. The red line shows the measured mole fraction. Note that there are some time periods when no measurements are available due to either calibration processes or, more rarely, failure of the monitoring instrumentation. For such periods, modelling results are not shown.

The Trainou (TRN) station (bottom subplot in Figs. 5 and A1) is far from the Paris agglomeration. In addition, the measurement inlet is at 180 m from the surface. It shows a diurnal cycle amplitude that is much smaller than at the other sites. In addition, the contribution from both anthropogenic and biogenic fluxes within the simulation domains is limited to a few ppm (difference between the blue and green curve). There are a few exceptions however, essentially when the wind blows from the North, i.e. from the Paris city, and transports CO₂ to the TRN rural site. The best examples are around 8 December and 23 December. For these particular cases, the measurements at TRN are significantly larger than the model. The underestimate by the model is not limited to these dates and there are significant discrepancies between the model and the measurements at this background site, in particular at the end of November and at the beginning of December.

The other sites are much closer to Paris and are then more affected by the fossil CO₂ emissions. At Gif-sur-Yvette (GIF) the largest mole fractions are observed when the wind is from the North-East, which is expected as the Paris city is in that direction.

An attempt at estimating Paris area CO₂ emissions

F. M. Bréon et al.

Title Page

Abstract

Introduction

Conclusions

References

Tables

Figures



Back

Close

Full Screen / Esc

Printer-friendly Version

Interactive Discussion



An attempt at estimating Paris area CO₂ emissions

F. M. Bréon et al.

Title Page

Abstract

Introduction

Conclusions

References

Tables

Figures



Back

Close

Full Screen / Esc

Printer-friendly Version

Interactive Discussion



There is also an impact of the wind, as the largest mole fractions are measured in low wind speed conditions. During the October–November period (Fig. A1), the wind is mostly from the South and South-West, thus not from the city, and there is a relatively good agreement between the modelled and measured mole fractions. In December, the wind direction is more variable, the fossil CO₂ signal appears much larger, and there are very significant differences between the measurements and the model estimates.

Gonesse (GON) is located to the North of the city, while Montgé-en-Goële (MON) is further away to the North-East. The shorter distance to the main source may explain the larger signal at the former station. The only cases when the expected anthropogenic contribution is small at GON (small difference between blue and green curve) is when the wind is from the North. For other wind directions, the modelled signal is strong (more than 10 ppm) and there are large differences between the measurements and the modelling results. During December, the measurements are most often larger than the model estimates. A similar observation can be made at MON. Surprisingly, the measurements are significantly larger than the modelling results, even when the wind blows from the North or North-East, i.e. when the Paris agglomeration contribution is negligible (3 December, 6–9 December, 22–23 December). For these cases, the most likely explanation is an underestimate of modelled CO₂ from the boundary conditions. Note that the modelled boundary conditions and the contribution from emissions outside Île-de-France (blue line) show a large increase of the mole fraction for these periods. One may then hypothesize that this increase is underestimated. The interpretation is that anthropogenic emissions from the Benelux area generate high concentrations that are underestimated in the boundary condition field that is used in our simulations.

The EIF site is at the top of the Eiffel tower, 300 m above the Paris city. There is then no expected signal variation with the wind direction. The wind speed for this station site is larger than for the other one, simply because it is higher in altitude. As EIF is in altitude, one expects atmospheric mixing between the surface emissions and the inlet, so that the measurements are representative of a larger area than e.g. MON and GON. Nevertheless there are some very significant differences between the model and the

An attempt at estimating Paris area CO₂ emissions

F. M. Bréon et al.

Title Page

Abstract

Introduction

Conclusions

References

Tables

Figures

◀

▶

◀

▶

Back

Close

Full Screen / Esc

Printer-friendly Version

Interactive Discussion



observations at EIF. The differences may be huge, larger than 30 ppm, even during the afternoon (24 October, 7 November, 3 December, 12 December). Clearly, our atmospheric modelling framework cannot properly represent the mole fraction time series at the EIF station, either because of strong local (sub grid cell) emissions, or because of atmospheric transport processes that are not properly represented, in particular concerning the vertical transport above the city.

The curves in Figs. 5 and A1 show very large temporal variations of CO₂ within a day. Further analysis confirms that the largest variations are observed during the night, when the mixing layer is shallow. The CO₂ mole fraction at the surface is then affected by local sources, and the concentration very much depends on the atmospheric vertical mixing, something that is difficult to accurately reproduce in the model. It is then clear that the night-time and morning measurements are not appropriate for the flux inversion, as inverting them would be too sensitive to atmospheric transport biases. This justifies our choice of selecting only hourly measurements between noon and 4 p.m. The time series discussed here show the daily averages of these measurements and modelled values as diamond symbols.

2.6 Discussion

Both the measurements and the modelling results show a large impact of the Paris area anthropogenic emissions on the CO₂ mole fractions at the 5 sites analysed here. The mole fraction increases over the modelled background depends on the wind speed and direction and a typical order of magnitude is 10 ppm. As expected, the signal is smaller for the rural station of TRN, which is further away from the city than the other sites. Many of the features in the measured time series are well reproduced by the modelling framework, which gives some confidence in its usefulness to improve the emission estimates.

There are also some significant differences between the measured and modelled mole fractions that cannot be explained just by inaccurate emission inventories. The most obvious such feature is the mole fraction underestimate in Northerly wind condi-

**An attempt at
estimating Paris area
CO₂ emissions**

F. M. Bréon et al.

Title Page

Abstract

Introduction

Conclusions

References

Tables

Figures

◀

▶

◀

▶

Back

Close

Full Screen / Esc

Printer-friendly Version

Interactive Discussion



tions when the MON and GON sites shall be little sensitive to the Île-de-France emissions. This observation strongly suggests that the boundary conditions that we use have biases with a typical magnitude that is similar to the impact of the Paris area emissions. Such boundary conditions errors may have a significant impact on the flux inversion results. On the other hand, one may expect that the errors in the boundary conditions are similar for all stations that are spatially close. It then suggests the use of gradients in the CO₂ mole fractions rather than the absolute value of CO₂ measurements in the inversion procedure.

The other feature is much larger errors at the EIF site than at the other stations. Clearly, the modelling of the atmospheric transport is inaccurate for this particular site. It may have detrimental impact on the emission estimates derived from atmospheric inversion. Finally, the forward simulations show that the TRN site is little sensitive to the Paris area emissions due to its location further away from the city than the other sites.

In the following, we shall then describe two attempts at inverting the Paris area emissions from the concentrations. The first one uses the 5 site records and relies on the boundary conditions provided by the model. The second one only uses the measurements from GON, MON and GIF that are near-surface stations in the near vicinity of the Paris city, and the flux inversion is based on the CO₂ mole fraction gradients between the upwind and downwind stations, which requires the selection of favourable wind conditions. The set-up is very similar for these two inversions and is described in the next section. The results for the inversion based on the 5 site measurements are discussed in Sect. 4; those for the inversion based on the gradients are in Sect. 5.

3 Flux inversion

3.1 Principles

We follow a linear Bayesian inversion approach with Gaussian error statistics to find the optimal surface fluxes (anthropogenic emissions and biogenic fluxes) and their uncertainties from a prior estimate of the fluxes and from the mole fraction measurements.

We call \mathbf{x} the state vector that gathers the scaling factors for the 6 hourly flux maps, \mathbf{x}_B its prior estimate, \mathbf{H} the matrix operator that relates state parameters and mole fraction variations according to our atmospheric transport model, \mathbf{y} the observed mole fractions (or mole fractions gradients), \mathbf{y}_F the simulated impact of the lateral boundary conditions and of the fluxes that are not accounted for in the state vector on these mole fractions, \mathbf{B} the uncertainty covariance matrix of \mathbf{x}_B , and \mathbf{R} the error covariance matrix of \mathbf{y} . These components are detailed in the next section.

The optimal solution is given by (Tarantola, 2005):

$$\mathbf{x}_A = \mathbf{x}_B + \left(\mathbf{B}^{-1} + \mathbf{H}^T \mathbf{R}^{-1} \mathbf{H} \right)^{-1} \mathbf{H}^T \mathbf{R}^{-1} (\mathbf{y} - \mathbf{y}_F - \mathbf{H} \mathbf{x}_B) \quad (1)$$

and its posterior error covariance matrix is

$$\mathbf{A} = \left(\mathbf{B}^{-1} + \mathbf{H}^T \mathbf{R}^{-1} \mathbf{H} \right)^{-1} \quad (2)$$

Note that \mathbf{A} does not depend on the actual measurement values, but varies (among other factors) with their temporal and spatial sampling.

3.2 State vector: \mathbf{x}

Both the anthropogenic and biogenic prior fluxes described in Sect. 2 show a large diurnal cycle that impacts the model simulations of CO_2 , and that is likely uncertain. It then appears useful to invert this cycle together with the flux mean value. However,

Title Page

Abstract

Introduction

Conclusions

References

Tables

Figures

◀

▶

◀

▶

Back

Close

Full Screen / Esc

Printer-friendly Version

Interactive Discussion



only CO₂ measurements during the early afternoon can reliably be used to estimate the fluxes and their information from CO₂ measurements about the daily cycle is rather poor. We limit the number of independent periods to 4 corresponding to the local times between 0–6 h, 6–12 h, 12–18 h, and 18–24 h, respectively.

For the fossil flux, we use independent scaling factors for each individual day in the state vector, which makes the number of corresponding variables amount to $30 \times 4 = 120$ for the 30 day period of the inversion. These scaling factors apply to the prior flux estimates derived from the AirParif inventory ($\lambda_{0-6}^i, \lambda_{6-12}^i, \lambda_{12-18}^i, \lambda_{18-24}^i$ with i between 1 and 30).

Similarly, we optimize scaling factors for the prior NEE from C-TESSSEL. The simulation domain shown in Fig. 1 is split into 3×3 large boxes, and we choose the same 6 h periods than for the anthropogenic fluxes to optimize scaling factors of NEE. However, we do not attempt a daily retrieval of NEE, so that we use a single scaling factor for optimizing monthly NEE each 6 h window over a 30 day inversion period. The number of variables to optimize NEE is therefore $3 \times 3 \times 4 = 36$. In the following, these NEE scaling factors are shown as $\alpha_{0-6}^X, \lambda_{6-12}^X, \alpha_{12-18}^X, \alpha_{18-24}^X$ where X is one of the 9 large boxes. One of the 9 boxes covers the Île-de-France region, the other ones are in the surrounding. In the *Inversion results* sections, we will analyse the inversion of NEE for the centre box ($X = C$) together with those for the anthropogenic emissions. The surrounding boxes provide some degree of freedom to the inversion system to adjust the likely biased boundary conditions.

Finally, there is one monthly variable (C_{Offset}) in the state vector to adjust a possible large scale offset on the modelled concentrations over the domain and 30 day period.

The state vector for the linear inversion has therefore $120 + 36 + 1 = 157$ variables. The prior estimate for C_{Offset} is 0 as the modelled is expected to reproduce the large-scale concentration with no bias, since CO₂ boundary conditions are from a global LMDZ inversion making use of global station observations during the same period than the inversions 30 day periods. All other components of the state vector represent scaling factors to the modelled fluxes and have therefore a prior value of 1.

An attempt at estimating Paris area CO₂ emissions

F. M. Bréon et al.

Title Page

Abstract

Introduction

Conclusions

References

Tables

Figures

◀

▶

◀

▶

Back

Close

Full Screen / Esc

Printer-friendly Version

Interactive Discussion



3.3 Measurements: y

The y vector contains the measurements that are used to constrain the flux inversion. As explained above, we only use the hourly measurements that have been acquired during the afternoon from noon to 4 p.m. local time. In addition, the measurements need to be representative of a relatively large area to reduce the sensitivity to local, unresolved, fluxes (e.g. below the atmospheric transport model resolution). This condition is not met when the wind speed is low. We therefore use for the inversion only the measurements that have been acquired with a wind speed larger than a given threshold. In the version of the inversion system used here, the threshold is set at 2 ms^{-1} . The wind speed is that analysed by the ECMWF at the location, height, and time of the observation. This criterion retains about 70 % of the potential measurements. Note that the wind generally increases with altitude so that a larger fraction of observations are considered valid at the tower sites (TRN and EIF) than at the others.

In Eq. (1) the mole fraction measurements y are corrected for the contributions that are not accounted for in the state vector (y_F). y_F are the modelled mole fraction accounting for the boundary conditions and anthropogenic fluxes outside Île-de-France (prescribed from the Edgar database). This contribution is shown as a blue line in Figs. 5 and A1.

One version of the inversion system uses the measured mole fractions at the 5 sites. Following the discussion of Sect. 2.6, the other version is based on the gradients between the stations in the borders of the city area, i.e. GIF, MON and GON: when the wind is from the South-West (upwind direction between 160 and 260°), GIF is considered as a background upwind from the city, and the corresponding y elements are the differences between the mole fractions measured at either MON or GON and that measured at GIF. Similarly, when the wind is from the North-East (upwind direction between 0 and 135°), MON is used as a background for the GIF or GON mole fraction measurements. For other wind directions, the measurements are not assimilated.

Title Page

Abstract

Introduction

Conclusions

References

Tables

Figures



Back

Close

Full Screen / Esc

Printer-friendly Version

Interactive Discussion



3.4 Prior flux uncertainties and error correlations: B

Although we separately invert the scaling factors of fossil CO₂ emissions for each day and each 6 h period, the uncertainties in these factors are correlated. We therefore attempt to assign correlations for the prior uncertainties, even though there is very limited information about these error correlations, based on several considerations: (i) the monthly budget for the AirParif inventory is generally stated to have an uncertainty of 20 % which is used here; (ii) we assume small positive correlations between the different 6 h windows; (iii) we assume stronger correlations from day to day for a given 6 h window; (iv) the a priori uncertainty of individual 6 h emission should have a typical order of 50 %.

Based on these considerations, we set, rather arbitrarily, prior error correlations to 0.4 for two adjacent time periods (e.g. 12–18 and 18–24) and to 0.2 for non-adjacent time period (e.g. 6–12 and 18–24). For successive days, we use an exponential decorrelation with a characteristic time T_{cor} . The correlation between the prior uncertainties of the fossil CO₂ emissions scaling factors is then the product of this exponential and the time correlation. For instance, the correlation between λ_{0-6}^5 and λ_{6-12}^9 is $0.4 \exp(-4/T_{\text{cor}})$. The results shown in this paper have been mostly obtained with a temporal correlation T_{cor} of 7 days, but other values, from 1 to 30 days, have been also tested. We have verified that such correlations define a proper definite positive correlation matrix. The desegregation of the assumed 20 % uncertainty for the monthly emission totals, based on these temporal correlations, results in a standard deviation of uncertainties for individual 6 h period of 33 % ($T_{\text{cor}} = 30$ days) to 50 % ($T_{\text{cor}} = 7$ days).

For the biogenic flux scaling factors, we set a relative prior uncertainty (standard deviation) close to 0.70 with some variations according to the box size (the variance varies inversely to the surface of the box), based on the numbers derived at 0.5° resolution in (Broquet et al., 2011). We do not assign any spatial/temporal correlation between the various biogenic scaling factors, i.e. between the 9 boxes or the 4 time periods. Similarly, there is no correlation in **B** between the prior uncertainties on the biogenic and

Title Page

Abstract

Introduction

Conclusions

References

Tables

Figures

◀

▶

◀

▶

Back

Close

Full Screen / Esc

Printer-friendly Version

Interactive Discussion



anthropogenic fluxes, neither between the offset mole fraction and the other parameters in the state vector. For C_{offset} , we assign an uncertainty of 5 ppm, corresponding to typical large scale variations of the mole fractions at the boundary conditions.

3.5 Observation error: \mathbf{R}

5 The measurements provided by the instrument are precise, certainly better than 0.3 ppm. However, the observation error that needs to be quantified here includes the representation error, the uncertainty in the spatial distribution of the fluxes, and the atmospheric transport modelling error that are difficult to assess (Broquet et al., 2013). This representation error is particularly important for the urban environment that is
10 discussed here. We deduce the observation error from the statistics of the difference between the measured and modelled mole fractions, both for the prior and posterior modelling, removing the uncertainties coming from the state vector (i.e. the fluxes). We only assess the CO_2 mole fraction differences during the afternoon. Based on this analysis, we use a 10 ppm observation error for the EIF station and 5 ppm for the other
15 sites.

If the observation errors between the various sites were uncorrelated, we should set larger errors for the inversion based on the gradients (by a factor of $\sqrt{2}$). The analysis of the time series shows that a significant fraction of the error is actually similar from site to site, which is consistent with the hypothesis that erroneous background
20 conditions drive the observation error. The statistics of the differences between the measured and modelled mole fraction gradients are much better (i.e. smaller) than for the absolute mole fraction values. Based on these statistics (see Figs. 10 and A7) we set the gradient observation error to 3 ppm.

Due to the complexity and misunderstanding of the processes underlying the obser-
25 vation error, that may lead to positive or negative correlations, we assume uncorrelated measurement errors (\mathbf{R} is diagonal).

An attempt at estimating Paris area CO_2 emissions

F. M. Bréon et al.

Title Page

Abstract

Introduction

Conclusions

References

Tables

Figures

◀

▶

◀

▶

Back

Close

Full Screen / Esc

Printer-friendly Version

Interactive Discussion



3.6 Operator matrix: \mathbf{H}

The operator matrix \mathbf{H} provides the link between the surface fluxes and the mole fraction measurements. It combines the spatio-temporal distribution of the fluxes from the AirParif inventory (or C-Tessel for biogenic fluxes) that is assumed and not modified through the inversion, the atmospheric transport by the Chimere model, and the sampling of the atmosphere at the instrument locations. Note that the AirParif inventory has a 1 h temporal resolution. The direct simulation ($\mathbf{H}\mathbf{x}$) uses the description of the emissions at this temporal resolution. Each element of the state vector, except for C_{Offset} , corresponds to the natural or anthropogenic surface flux for a larger time period. We use the Chimere model driven by the ECMWF meteorology to compute the impact of each surface flux to the atmospheric concentrations (156 simulations). The 4-D mole fraction fields are then sampled at the place and time of the atmospheric observations. For the *gradients* version of the inversion, the sampling is set as the difference between the simulated mole fractions at the two sites that are considered when the conditions described in Sect. 3.3 are verified. By definition of this parameter, the column of the \mathbf{H} matrix that corresponds to C_{Offset} is set to 0 for the gradient version of the inversion, and 1 ppm for the other version.

4 Results

We present below the results obtained with the first version of the inversion system that uses the mole fraction measurements at all five sites. Section 5 shows the results based on the concentration gradients between the 3 sites that are in the near surrounding of the Paris city.

4.1 Daily fossil fuel CO_2 emissions

Figure 6 shows the daily anthropogenic fluxes inferred by the inversion. Here, we have aggregated the 4 6 h periods as well as their uncertainty, accounting for the error cor-

Title Page

Abstract

Introduction

Conclusions

References

Tables

Figures

◀

▶

◀

▶

Back

Close

Full Screen / Esc

Printer-friendly Version

Interactive Discussion



relations between the periods. Although the inversion tool controls scaling factors, we show here the resulting fluxes expressed in Mt CO₂ per day. The blue line and shaded area show the prior fluxes and their uncertainties. There is a clear weekly cycle (less emissions during the week-end). One may also note a shift in emission between 29 October and 1 November that corresponds to a change of month and therefore a different dataset in the AirParif inventory. The Airparif inventory includes a profile for October. For November and December, Airparif recommends the use of the January emission profile. The red symbols show the anthropogenic emission derived from the inversion together with its uncertainty. The theoretical posterior uncertainties are reduced by a factor of typically two from their prior values. The day-to-day variations of the posterior fluxes are, however, surprisingly large. The largest flux corrections can be easily traced back to measured mole fractions larger than the prior modelled values: at the beginning of the first period, mole fraction measurements are much larger than the prior, in particular at GON and EIF. Note that winds are rather small during the first days (below the 2 ms⁻¹ threshold), so that the MON and GON measurements have not been used for the inversion. 3 December is another day with low wind speeds, but the MON observation meets the wind speed threshold and is much larger than the prior. The EIF measurement is also very large compared to the simulation. Similar conditions appear for 21 December and only the EIF measurements drive the inversion. These observations suggest that low wind speeds lead to unreliable inversion results in this configuration, likely because of unresolved local sources influencing the sites, even with the 2 ms⁻¹ threshold that we use for selecting observations. At the other extreme, the inversion infers a very low flux for 4 December. This can be traced back to measurements that are smaller than the prior by about 10 ppm at all operating sites (GIF was down). There is nothing specific for the wind on this particular day while the background (blue line) shows a local maximum that does not appear in any of the station site measurements. One may then blame the boundary conditions for the misfit during that particular event.

An attempt at estimating Paris area CO₂ emissions

F. M. Bréon et al.

Title Page

Abstract

Introduction

Conclusions

References

Tables

Figures

◀

▶

◀

▶

Back

Close

Full Screen / Esc

Printer-friendly Version

Interactive Discussion



An attempt at estimating Paris area CO₂ emissions

F. M. Bréon et al.

Title Page

Abstract

Introduction

Conclusions

References

Tables

Figures

◀

▶

◀

▶

Back

Close

Full Screen / Esc

Printer-friendly Version

Interactive Discussion



We also tested similar inversions using different correlation times (T_{cor}) in the range of the synoptic to seasonal time scales that drives the emission variability. With a 1 day correlation time, rather than 7 days used so far, there are days with little or no flux constrain by the observations, while there is no smoothing of the day-to-day variability, resulting in an even larger spread (not shown). The low estimate that is obtained on 4 December above becomes negative, which is unrealistic, and the largest daily values are close to $0.5 \text{ Mt CO}_2 \text{ day}^{-1}$. At the other extreme, a 30 day correlation time leads to much smoother results (See Fig. A3). Most of the daily-optimized flux estimates remain within the prior uncertainty range. The weekly cycle is apparent in the posterior fluxes but is driven by the prior rather than the observations.

4.2 Diurnal cycle

Figure 7 shows the monthly mean flux estimates for the Île-de-France region for the various 6 h periods. It shows the results of the inversion for the anthropogenic emissions, the NEE, as well as the total. Note that the total estimate is necessarily the sum of the biogenic and anthropogenic fluxes. Conversely, the uncertainty range is not a simple sum as it accounts for the correlations between NEE and fossil CO₂ emission errors, in the **A** matrix.

As expected, the flux inversion has very little impact on the fluxes for the 0–6 and 18–24 periods. This is because we only use measurements between noon and 4 p.m., which are little affected by the emissions and sinks from these nocturnal time periods. On the other hand, the anthropogenic flux uncertainty is strongly reduced (by more than a factor of 3) for the 6–12 and 12–18 time periods, when measurements are assimilated. The anthropogenic flux estimate shows limited change from its prior estimate and it remains within the prior uncertainty. In this set of inversion, the largest change from the prior estimate is for the NEE, for the period 12–18 h during the November–December period. One notes that the posterior estimate of the afternoon NEE is slightly positive from a strong negative value, and outside of the prior uncertainty range.

An attempt at estimating Paris area CO₂ emissions

F. M. Bréon et al.

Title Page

Abstract

Introduction

Conclusions

References

Tables

Figures

◀

▶

◀

▶

Back

Close

Full Screen / Esc

Printer-friendly Version

Interactive Discussion



The uncertainties on the total flux (blue) are similar to what is expected for an uncorrelated sum of the biogenic and fossil CO₂ fluxes uncertainties, i.e. a quadratic sum. It is slightly smaller for the afternoon period due to a negative correlation (−0.35) between the posterior uncertainties of NEE and fossil CO₂ fluxes for both 30 day periods.

Other periods show much smaller correlations. These numbers indicate that the observation sampling should be able to separate NEE from fossil CO₂ fluxes in the inversion. Although a given measurement cannot trace the origin of the mole fraction excess, the assigned biogenic and anthropogenic flux errors have different spatial and temporal patterns which are exploited by the inversion system to attribute the mole fraction signal to specific sectors.

Of note is the peculiarity of NEE during the 6–12 h period of October–November (Fig. A4). The NEE flux and uncertainty range are very close to zero. This corresponds to the total NEE of the 6 h period. The flux is generally positive (emission) during the early hours, and negative (sink) later on within this 6 h period. The inversion does correct the value of a_{6-12}^C (the posterior value is 1.36 for a prior value of 1) and therefore the amplitude of the NEE cycle. It has however little impact on the total flux during the entire 6 h period, so that optimized NEE values remains much smaller than the anthropogenic flux or the biogenic fluxes during the other time periods.

4.3 Impact of the flux correction on the CO₂ mole fractions

Figures 8 and A5 show scatter plots of measured vs. modelled mole fractions. The first line of the plots on each of these figures shows the modelled mole fractions from the domain boundaries and the fossil CO₂ emission outside Île-de-France (blue lines in Fig. 5, y_F in Eq. 1) against the measurement. This constitutes the contribution to the mole fraction that is not optimized by the inversion. For the TRN tall tower site (first column) that is far from Paris, there is a fairly good agreement between measured and modelled mole fractions during the first period (October–November, in Appendix). It is interesting to note that the second period (November–December) shows a much larger observed variability of CO₂ at TRN than the first one. This variability is well reproduced

by the model (correlation is 0.81) although the slope of the best linear relationship is clearly smaller than 1. Similarly, the GIF site shows a much larger variability during the second period than during the first. This is well explained by the fact that, during the first period, the wind is mostly from the South and South-West so that the GIF site is not significantly affected by the Paris city emission. For other cases, there is a large spread in the scatter plots, which is expected as the Paris city emissions affect the measurements but not the modelled values from the domain boundaries and emissions outside Île-de-France.

The second line shows simulated CO₂ from transported prior NEE and fossil CO₂ fluxes (i.e. those that are optimized through the inversion) against measured mole fractions corrected for the background (i.e. that shown on the Y-axis of the first line). Although there is a large spread, the correlation is significant, which shows that the transport model and the prior flux set up have altogether some ability to reproduce the observed variability. During the October–November period, the biases are fairly small at all sites except EIF (top of Eiffel tower); during the November–December period, the comparison show much larger negative biases up to −13 ppm at EIF and −9 ppm at MON. The standard deviation of the measurement-model difference varies with the sites and period, between 3.1 and 15.3 ppm. They are larger for the later period than for the earlier one and smaller at TRN than for the sites that are closer to Paris.

After the inversion (third line) the agreement is significantly improved, although there are sites where either the bias or the standard deviation of the model-data misfit is degraded. The change in bias between the prior and posterior values is mostly explained by the optimized offset mole fraction C_{Offset} . It is 1.8 ppm for the October–November period and 5.1 ppm for the November–December period. Thus, the inversion system corrects for the measurement biases by adjusting the large scale offset rather than the fossil CO₂ emissions or NEE fluxes. Note that, for both periods, the bias at EIF is much larger than for the other sites. Also, the hypothesis of a large-scale constant and uniform bias in the modelled mole fractions, underlying the use of C_{Offset} within the inversion, is not compatible with the observations at TRN, a site which is mostly outside

An attempt at estimating Paris area CO₂ emissions

F. M. Bréon et al.

Title Page

Abstract

Introduction

Conclusions

References

Tables

Figures

◀

▶

◀

▶

Back

Close

Full Screen / Esc

Printer-friendly Version

Interactive Discussion



An attempt at estimating Paris area CO₂ emissions

F. M. Bréon et al.

Title Page

Abstract

Introduction

Conclusions

References

Tables

Figures

◀

▶

◀

▶

Back

Close

Full Screen / Esc

Printer-friendly Version

Interactive Discussion



of the Paris agglomeration influence. After the inversion, the bias at TRN is larger than in the prior. Although the inversion interprets biases as resulting from a large-scale signal to be corrected by optimization of C_{offset} , this does not seem consistent with the measurements. The origin of the discrepancy lies in the very large biases at EIF. This confirms that the atmospheric transport modelling does not reproduce the mole fractions properly at the top of the Eiffel tower. There seems to be specific features in the atmospheric vertical transport over the Paris city or local emissions beneath the EIF tower location that are not well represented in the model used in this study, and that lead to higher mole fractions at this location.

After the inversion, the standard deviation is between 3.7 and 5.2 ppm except for EIF where it reaches 13.4 ppm. The standard deviation is always significantly larger than the bias, so that the RMS error is similar to the standard deviation. Again, the EIF site appears poorly represented compared to the other sites. We have therefore attempted an inversion excluding the measurements from that particular site. The inversion results appear more realistic: C_{Offset} is then 1.2 ppm and 4.5 ppm for the two 30 day periods (compared to 1.8 and 5.1 when EIF is assimilated). The statistics at the various sites are slightly improved, but the daily flux retrievals (as those shown in Fig. 6) are still highly variable.

5 Results for the inversion based on concentration the gradients

We now present the inversion results where the input data are the spatial gradients between two measurement sites with a “background” reference site chosen based on the wind direction (see Sect. 3.3). Figures 9 and A6 show the time series of these differences (only the afternoon mean are shown). The prior value is almost always positive, as shall be expected because the reference is chosen upwind of the Paris agglomeration. There are a few exceptions, as on 22 December at GON. On this particular date, the reference chosen is MON according to the wind direction. Further investigation demonstrated that this unexpected behaviour is linked to a large spatial gradient of the

CO₂ concentration generated by anthropogenic emissions over the Benelux accounted for in the Edgar inventory transported by the Chimere model (y_F in Eq. 1). Interestingly, the observations confirm the sign and order of magnitude of the gradient that is modelled with our setup that uses crude anthropogenic emissions outside Île-de-France.

5 The scatter plots of Fig. 10 confirm that the modelling of gradients is far more consistent with observations than that of the absolute mole fractions (Fig. 8). Indeed, the prior model-measurement correlations range from 0.47 and 0.82 for the latter, when they are from 0.83 to 0.93 for the former.

Although the modelling expects mostly positive mole fraction gradients, the observed values can be negative both at GON and GIF. At GON, negative values are found only in Northerly wind conditions, i.e. when MON is used as a reference. As GON is in the northern part of the Paris agglomeration, one expects a smaller signal than for southerly wind conditions. The negative gradients values using GIF as a reference, in particular that of 3 December are more surprisingly and we could not find a valid explanation for them.

As expected, the posterior estimates of the mole fractions (blue symbols) are closer to the observations (red) than the prior (green). This is better shown in Fig. 10, which confirms that the statistics on the mole fraction gradients have been significantly improved through the inversion. Note however that the standard deviation for the MON site (when GIF is used as a reference) is slightly degraded from the prior value of 2.0 ppm. After the inversion, the correlation between optimized and observed CO₂ gradients for all three stations is larger than 0.90. For the other time period shown in the Appendix (Fig. A7), the correlation statistics are not as good. However, this is due to a lower variability of the gradients, and the posterior standard deviations are 2.3, 2.7 and 2.3 ppm for the three sites, and are then similar as the values shown in Fig. 10.

25 The inverted daily fluxes based upon the gradient inversion are shown in Fig. 11. The uncertainty reduction is significant for all the days of the two time periods and a typical order of magnitude is a factor of 2, like in the inversion of absolute mole fractions at each site. The emission uncertainty is reduced even for days with no usable mea-

An attempt at estimating Paris area CO₂ emissions

F. M. Bréon et al.

Title Page

Abstract

Introduction

Conclusions

References

Tables

Figures

◀

▶

◀

▶

Back

Close

Full Screen / Esc

Printer-friendly Version

Interactive Discussion



surements (i.e. when the wind direction is not within any of the two ranges defined in Sect. 3.3) due to the temporal correlation of the uncertainties and thus of the corrections applied to the prior (Sect. 3.4). The deviations of the flux estimate from the prior follow the gradient observation deviation from the model (Fig. 9). These deviations are mostly negative, although they are positive for a few days during both time periods. For the November–December period, the posterior emission estimates are within the bounds of the prior uncertainty range. On the other hand, the posterior estimate is much lower than the prior flux during the second half of the October–November period (Fig. 11, top). Interestingly this period (1 November to 20 November 2010) was very mild (Meteo France, 2010) which may explain that heating sector emission were well below the AirParif inventory values for that period. During this season, according to the AirParif inventory, the heating sector (commercial and residential) amounts to more than 50 % of the emission, so that the total emission is highly sensitive to temperature. Note that AirParif recommends the use of the January inventory for both November and December. As the temperatures are generally milder during October than January, one may expect that the inventory is larger than the true fluxes during October, which may explain the negative correction to the fluxes during that period.

Figure 12 shows the 30 day flux estimates, prior and posterior, for each of the 6 h periods. As for the results shown in Sect. 4, the inversion has little impact on the fluxes for the 0–6 h and 18–24 h periods. On the other hand, the impact is strong for the 6–12 h and 12–18 h periods. Although the inversion based on the gradients uses less independent observation than the full inversion does (less sites, a data selection based on wind direction), the impact of this setup on the flux estimates is larger. One reason is that we have set a lower uncertainty for the gradient than for the mole fractions (Sect. 3.5). Another reason is that many measurements that are not used here, in particular those at TRN, but also those crosswind of the Paris plume in the vicinity of the agglomeration, are little sensitive to the Île-de-France emissions so that they bring little information to the inversion when assimilating absolute mole fractions. Clearly, the

An attempt at estimating Paris area CO₂ emissions

F. M. Bréon et al.

Title Page

Abstract

Introduction

Conclusions

References

Tables

Figures

◀

▶

◀

▶

Back

Close

Full Screen / Esc

Printer-friendly Version

Interactive Discussion



setup of the inversion based on the gradient retains the observations that do constrain the Paris agglomeration emissions, and should be recommended for future studies.

6 Discussion and conclusions

This paper is a first attempt at estimating the Paris area emissions from measurements of atmospheric CO₂ mole fractions and prior flux knowledge. There is obviously room for improvement in several aspects of the inversion system: the number and spatial distribution of the monitoring stations, the atmospheric transport model including the use of an urban scheme, the setting of concentration at the simulation domain boundaries, the definition of the emissions outside Île-de-France, the definition of the control vector, etc. However, first conclusions of broad implications beyond this first attempt can be drawn, that should guide further inverse modelling developments for Paris and other cities.

The analysis of the CO₂ time series shows significant differences between the measured and modelled mole fractions upwind from the Paris city. These differences demonstrate that the simulated mole fraction at the domain boundaries may be off by several ppm. Although the number of cases is limited, it seems that the boundary concentrations are significantly underestimated when the wind is from the North or North-East (Benelux). These large uncertainties on the domain boundaries suggest applying the inversion not on the measurements themselves, but rather on the spatial gradients from the measurements at the upwind stations as was done in Sect. 5. Indeed, the measurement-model agreement is much better for the gradients (Fig. 10) than it is for the direct values (Fig. 8). It confirms that the large-scale pattern of CO₂ mole fraction, which is not related to the Île-de-France fluxes, is not properly modelled. The information provided by our five-site network does not allow optimizing the structure of the CO₂ boundary conditions, which is directly prescribed by a coarse scale global inversion. Exploiting the distant sites currently operational in Europe would unlikely improve this situation. In this context, the inversion based upon gradients as presented in Sect. 5

An attempt at estimating Paris area CO₂ emissions

F. M. Bréon et al.

Title Page

Abstract

Introduction

Conclusions

References

Tables

Figures



Back

Close

Full Screen / Esc

Printer-friendly Version

Interactive Discussion



5 appears more reliable than those of Sect. 4 so that this setup should be our base-
line for future improvements. However, both measurements and atmospheric transport
simulations indicate that the CO₂ mole fraction signal generated by distant sources
outside the Chimere model domain has some spatial structures. As a consequence,
distant sources and sink do impact the inversion, even when using the concentration
gradients, although the resulting biases on the retrieved fluxes are very much reduced
compare to the inversion setup of Sect. 4.

10 The drawback of using the gradient is a reduction in the number of observations,
in particular with the current monitoring network that only samples a fraction of possi-
ble wind directions. Nevertheless, although the number of observations is very much
reduced, our inversion system based on the gradient indicates significant uncertainty
reductions. The smaller observation error on the gradients, compared to the absolute
mole fractions, allows assigning smaller values in the **R** vector, which leads to a larger
constrain by the available observations. It must also be noted that we assumed a 7
15 days correlation length for the anthropogenic emissions, so that our system shows flux
uncertainty reductions, even on days with no valid observation (the flux is constrained
by observation of the previous or following days).

20 The setting of correlation length is therefore essential for the inversion. Although the
results in this paper are mostly derived with a 7 days correlation length, this is a some-
what arbitrary choice, and the results are significantly affected when using different
values. In particular, a much shorter value (1 day) leads to very large variations in the
posterior daily emissions. For such short correlation length, the days with no valid ob-
servations show a posterior emission that is close to the prior value whereas the flux
change (from prior to posterior) is large for the days with observations. Further work
25 should be devoted to the assignment of objective correlation lengths based on the pro-
cesses that lead to emission uncertainties. The meteorology (temperature) impacts the
emission with a time scale that is consistent with synoptic events (close to a week); the
impact of specific events such as holidays, commemorations or strikes have a much

An attempt at estimating Paris area CO₂ emissions

F. M. Bréon et al.

[Title Page](#)[Abstract](#)[Introduction](#)[Conclusions](#)[References](#)[Tables](#)[Figures](#)[Back](#)[Close](#)[Full Screen / Esc](#)[Printer-friendly Version](#)[Interactive Discussion](#)

shorter time scale, while inventory biases linked to e.g. the emission factors have an impact on the fluxes on time scales of months or even larger.

Our analysis also indicates model-measurement discrepancies at the EIF site, i.e. at the top of the Eiffel tower, that are much larger than at other sites. This is somewhat surprising as measurement inlet in altitude should insure a larger representativeness than at the surface sites and less sensitivity to local, poorly represented, emissions. Usually, tall tower based measurements are preferred to those at the surface for the estimate of biogenic fluxes. EIF is located close to the centre of the Paris city and is therefore affected by stronger local emissions than the other sites used in this paper. There is a strong need for an analysis of the atmospheric processes that link the surface fluxes to the concentrations at the top of the Eiffel tower (urban canopy roughness, heat island effects, heterogeneity of the local sources). At present, our mesoscale atmospheric transport model cannot reconcile the measurements at the top of the tower to those at the surface in the vicinity of the city, given our set of surface fluxes and inversion settings. A temporary fix has been to disregard the measurements from the EIF site in a best attempt at inverting the Île-de-France CO₂ fluxes. However, our inability to reproduce the EIF mole fraction measurements cast doubts on the quality of the modelling at the other sites. Indeed, if the atmospheric transport model does not properly simulate the atmospheric vertical transport between the surface and an inlet at 300 m in altitude, it likely misrepresent the link between surface fluxes and atmospheric mole fractions. Conversely, the large modelling errors at EIF may be related to its urban location (and to the strong influence of local urban sources) and this would raise concerns regarding the ability to exploit urban measurements, and therefore to solve for the spatial distribution of the fluxes within the urban area.

The largest differences between the measured and modelled concentrations occur for low wind speeds. For this reason, we have chosen a 2 ms⁻¹ wind speed threshold below which the measurements are not used in the inversion. A larger threshold rejects further observations, and reduces the range of inverted daily fluxes. The choice of the threshold is clearly arbitrary and we have refrained from using a large one to clearly

An attempt at estimating Paris area CO₂ emissions

F. M. Bréon et al.

Title Page

Abstract

Introduction

Conclusions

References

Tables

Figures

◀

▶

◀

▶

Back

Close

Full Screen / Esc

Printer-friendly Version

Interactive Discussion



An attempt at estimating Paris area CO₂ emissions

F. M. Bréon et al.

[Title Page](#)[Abstract](#)[Introduction](#)[Conclusions](#)[References](#)[Tables](#)[Figures](#)[◀](#)[▶](#)[◀](#)[▶](#)[Back](#)[Close](#)[Full Screen / Esc](#)[Printer-friendly Version](#)[Interactive Discussion](#)

demonstrate the impact of a few situations with low wind-speed. There are several hypothesis for the poor modelling at low wind speed, including larger representativity errors of subgrid patterns, or larger errors in vertical mixing modelling. However, such issues are continuous and there is no indication that the modelling errors disappear between e.g. 2 and 3 ms⁻¹. Thus, further rejection of low wind-speed observations may hide the deficiencies in the atmospheric transport without improving the flux inversion.

We also stress that our analysis is based on measurements during the late fall period. This is a favourable case for the inversion of fossil fuel CO₂ emissions as there is less interference with the biogenic fluxes (Pataki et al., 2007). During spring and summer, the NEE is much larger (in absolute value) and also more uncertain. In fact, during May, the biogenic sink is likely larger than the anthropogenic emissions within Île-de-France. Individual mole fraction measurements cannot distinguish the origin of the concentration signal while the uncertainties on the biogenic fluxes are larger than those on the anthropogenic fluxes. The gradient set-up is designed to also minimize this interference of biogenic flux with the constraint on anthropogenic fluxes. Indeed, the theoretical posterior uncertainties indicate little correlations between the retrieved NEE and anthropogenic emissions. However, these results are based on strong assumptions such as the spatial and temporal distributions of the NEE fluxes are known within large areas. Therefore, in the real world, the inversion may still attribute some flux changes that are necessary to fit the concentrations to the biogenic rather than anthropogenic fluxes. It is certainly possible to estimate independently the biogenic and fossil fluxes from a large set of measurements but a successful inversion relies on an accurate description of the spatial and temporal distribution of both. A successful anthropogenic emission inversion still requires significant efforts for describing the biogenic fluxes and the use of additional tracers such as ¹⁴C to distinguish fossil fluxes and biogenic emissions. One future direction is thus to use a more realistic NEE model over the Paris area, that could be calibrated upon local eddy covariance observations (e.g. the method used in Gerbig et al., 2003) and satellite land cover and vegetation activity.

daily cycle that should rely on inventories. Thus, again, the top-down emission estimate is currently not independent from the bottom-up inventory.

Although the inversion procedure provides a posterior uncertainty estimate, one should use such uncertainty with caution. Indeed, the mathematical framework used here relies on a number of hypotheses, some of which are crude approximations of the reality (such as the spatial and temporal correlations in the flux uncertainties or the unbiased atmospheric transport modelling). The impact of these assumptions has not been quantified. Although we have no “truth” to benchmark our inversion, and there are not even enough measurement sites to perform “leave-one-out” tests, one can perform some sanity checks on the results. One sanity check is the comparison of the measured and modelled mole fractions (Figs. 8 and 10). The analysis of these figures confirms the ability of our inversion set-up to model the concentration gradients much better than the individual absolute measurements. Nevertheless, we note that the posterior misfit (≈ 2.5 ppm) is still a significant fraction of the signal that is analysed (10–20 ppm). The crucial question is whether the atmospheric modelling error is random or a bias and we have no element to answer that question. The other sanity check consists in analysing the validity of the retrieved daily fluxes (Fig. 11). In this respect, the daily fluxes show day-to-day variations that are suspicious, although not refutable at this stage. A result that points in favour of the flux inversions shown here is the significant reduction from the prior during a period with temperatures above the seasonal normal, and the negative correction of the emissions during November from the prior value that is based on an inventory simulating January emissions. A single such event is certainly not sufficient to validate the inversion system, however. We shall apply the same inversion setup to more than a year of measurements and analyse the results with respect to the temperature anomaly or other short-term event that may have a significant influence on the Île-de-France CO₂ emissions. More measurement sites are needed to better evaluate the skill of the inversion. The deployment of a network of 5 sites around Paris within the framework of the CarboCount-City project will help in this direction. A longer-

An attempt at estimating Paris area CO₂ emissions

F. M. Bréon et al.

Title Page

Abstract

Introduction

Conclusions

References

Tables

Figures

◀

▶

◀

▶

Back

Close

Full Screen / Esc

Printer-friendly Version

Interactive Discussion



term task consists in improving the atmospheric transport modelling within the city so that the measurement from the Eiffel tower top can be used in the inversion system.

Acknowledgements. This study was conducted within the ANR CO₂-Megaparis project and was made possible thanks to funding from the CarboCount and CarboCount-city KIC projects that are co-funded by the Climate KIC program of the European Institute of Technology. We thank Lin Wu and Isabelle Pison for assistance as well as all the developers of the AirParif inventory. Grégoire Broquet acknowledges funding and support from the *Chaire industrielle BridGES*, a joint research program between Thales Alenia Space, Veolia and the tutelary institutions of LSCE.

References

- Boussetta, S., Balsamo, G., Beljaars, A., Panareda, A. A., Calvet, J. C., Jacobs, C., van den Hurk, B., Viterbo, P., Lafont, S., Dutra, E., Jarlan, L., Balzarolo, M., Papale, D., and van der Werf, G.: Natural land carbon dioxide exchanges in the ECMWF integrated forecasting system: implementation and offline validation, *J. Geophys. Res.-Atmos.*, 118, 5923–5946, doi:10.1002/Jgrd.50488, 2013.
- Broquet, G., Chevallier, F., Rayner, P., Aulagnier, C., Pison, I., Ramonet, M., Schmidt, M., Vermeulen, A. T., and Ciais, P.: A European summertime CO₂ biogenic flux inversion at mesoscale from continuous in situ mixing ratio measurements, *J. Geophys. Res.-Atmos.*, 116, D23303, doi:10.1029/2011jd016202, 2011.
- Broquet, G., Chevallier, F., Bréon, F.-M., Kadyrov, N., Alemanno, M., Apadula, F., Hammer, S., Haszpra, L., Meinhardt, F., Morguí, J. A., Necki, J., Piacentino, S., Ramonet, M., Schmidt, M., Thompson, R. L., Vermeulen, A. T., Yver, C., and Ciais, P.: Regional inversion of CO₂ ecosystem fluxes from atmospheric measurements: reliability of the uncertainty estimates, *Atmos. Chem. Phys.*, 13, 9039–9056, doi:10.5194/acp-13-9039-2013, 2013.
- Chevallier, F., Ciais, P., Conway, T. J., Aalto, T., Anderson, B. E., Bousquet, P., Brunke, E. G., Ciattaglia, L., Esaki, Y., Frohlich, M., Gomez, A., Gomez-Pelaez, A. J., Haszpra, L., Krummel, P. B., Langenfelds, R. L., Leuenberger, M., Machida, T., Maignan, F., Matsueda, H., Morgui, J. A., Mukai, H., Nakazawa, T., Peylin, P., Ramonet, M., Rivier, L., Sawa, Y., Schmidt, M., Steele, L. P., Vay, S. A., Vermeulen, A. T., Wofsy, S., and Worthy, D.: CO₂

An attempt at estimating Paris area CO₂ emissions

F. M. Bréon et al.

Title Page

Abstract

Introduction

Conclusions

References

Tables

Figures

◀

▶

◀

▶

Back

Close

Full Screen / Esc

Printer-friendly Version

Interactive Discussion



An attempt at estimating Paris area CO₂ emissions

F. M. Bréon et al.

Title Page

Abstract

Introduction

Conclusions

References

Tables

Figures

◀

▶

◀

▶

Back

Close

Full Screen / Esc

Printer-friendly Version

Interactive Discussion



- surface fluxes at grid point scale estimated from a global 21 year reanalysis of atmospheric measurements, *J. Geophys. Res.-Atmos.*, 115, D21307, doi:10.1029/2010jd013887, 2010.
- Ciais, P., Bousquet, P., Freibauer, A., and Naegler, T.: Horizontal displacement of carbon associated with agriculture and its impacts on atmospheric CO₂, *Global Biogeochem. Cy.*, 21, Gb2014, doi:10.1029/2006gb002741, 2007.
- Duren, R. M. and Miller, C. E.: COMMENTARY: measuring the carbon emissions of megacities, *Nat. Clim. Change*, 2, 560–562, 2012.
- EDGAR: European Commission, Joint Research Centre (JRC)/Netherlands Environmental Assessment Agency (PBL), Emission Database for Global Atmospheric Research (EDGAR), release version 4.2, available at: <http://edgar.jrc.ec.europa.eu> (last access: 9 April 2014), 2011.
- Gerbig, C., Lin, J. C., Wofsy, S. C., Daube, B. C., Andrews, A. E., Stephens, B. B., Bakwin, P. S., and Grainger, C. A.: Toward constraining regional-scale fluxes of CO₂ with atmospheric observations over a continent: 1. observed spatial variability from airborne platforms, *J. Geophys. Res.-Atmos.*, 108, 4756, doi:10.1029/2002jd003018, 2003.
- Gurney, K. R., Law, R. M., Denning, A. S., Rayner, P. J., Baker, D., Bousquet, P., Bruhwiler, L., Chen, Y. H., Ciais, P., Fan, S., Fung, I. Y., Gloor, M., Heimann, M., Higuchi, K., John, J., Maki, T., Maksyutov, S., Masarie, K., Peylin, P., Prather, M., Pak, B. C., Randerson, J., Sarmiento, J., Taguchi, S., Takahashi, T., and Yuen, C. W.: Towards robust regional estimates of CO₂ sources and sinks using atmospheric transport models, *Nature*, 415, 626–630, doi:10.1038/415626a, 2002.
- Gurney, K. R., Razlivanov, I., Song, Y., Zhou, Y. Y., Benes, B., and Abdul-Massih, M.: Quantification of fossil fuel CO₂ emissions on the building/street scale for a large US city, *Environ. Sci. Technol.*, 46, 12194–12202, doi:10.1021/Es3011282, 2012.
- Lac, C., Donnelly, R. P., Masson, V., Pal, S., Riette, S., Donier, S., Queguiner, S., Tanguy, G., Ammoura, L., and Xueref-Remy, I.: CO₂ dispersion modelling over Paris region within the CO₂-MEGAPARIS project, *Atmos. Chem. Phys.*, 13, 4941–4961, doi:10.5194/acp-13-4941-2013, 2013.
- Lauvaux, T., Pannekoucke, O., Sarrat, C., Chevallier, F., Ciais, P., Noilhan, J., and Rayner, P. J.: Structure of the transport uncertainty in mesoscale inversions of CO₂ sources and sinks using ensemble model simulations, *Biogeosciences*, 6, 1089–1102, doi:10.5194/bg-6-1089-2009, 2009.

An attempt at estimating Paris area CO₂ emissions

F. M. Bréon et al.

Title Page

Abstract

Introduction

Conclusions

References

Tables

Figures

◀

▶

◀

▶

Back

Close

Full Screen / Esc

Printer-friendly Version

Interactive Discussion



- Lauvaux, T., Schuh, A. E., Uliasz, M., Richardson, S., Miles, N., Andrews, A. E., Sweeney, C., Diaz, L. I., Martins, D., Shepson, P. B., and Davis, K. J.: Constraining the CO₂ budget of the corn belt: exploring uncertainties from the assumptions in a mesoscale inverse system, *Atmos. Chem. Phys.*, 12, 337–354, doi:10.5194/acp-12-337-2012, 2012.
- 5 Levin, I., Hammer, S., Eichelmann, E., and Vogel, F. R.: Verification of greenhouse gas emission reductions: the prospect of atmospheric monitoring in polluted areas, *Philos. T. Roy. Soc. A*, 369, 1906–1924, doi:10.1098/rsta.2010.0249, 2011.
- Lopez, M., Schmidt, M., Delmotte, M., Colomb, A., Gros, V., Janssen, C., Lehman, S. J., Mon-
delain, D., Perrussel, O., Ramonet, M., Xueref-Remy, I., and Bousquet, P.: CO, NO_x and
10 ¹³CO₂ as tracers for fossil fuel CO₂: results from a pilot study in Paris during winter 2010, *Atmos. Chem. Phys.*, 13, 7343–7358, doi:10.5194/acp-13-7343-2013, 2013.
- McKain, K., Wofsy, S. C., Nehrkorn, T., Eluszkiewicz, J., Ehleringer, J. R., and Stephens, B. B.:
Assessment of ground-based atmospheric observations for verification of greenhouse
gas emissions from an urban region, *P. Natl. Acad. Sci. USA*, 109, 8423–8428,
15 doi:10.1073/Pnas.1116645109, 2012.
- Menut, L., Bessagnet, B., Khvorostyanov, D., Beekmann, M., Blond, N., Colette, A., Coll, I.,
Curci, G., Foret, G., Hodzic, A., Mailler, S., Meleux, F., Monge, J.-L., Pison, I., Siour, G., Tur-
quety, S., Valari, M., Vautard, R., and Vivanco, M. G.: CHIMERE 2013: a model for regional
atmospheric composition modelling, *Geosci. Model Dev.*, 6, 981–1028, doi:10.5194/gmd-6-
20 981-2013, 2013.
- Meteo France: [http://www.meteofrance.fr/web/comprendre-la-meteo/climat-passe-et-futur/
bilans-climatiques/bilan-2010/bilan-de-lautomne-2010](http://www.meteofrance.fr/web/comprendre-la-meteo/climat-passe-et-futur/bilans-climatiques/bilan-2010/bilan-de-lautomne-2010), Retrieved on 23 November 2013,
2010.
- Nehrkorn, T., Henderson, J., Leidner, M., Mountain, M., Eluszkiewicz, J., McKain, K., and
Wofsy, S.: WRF simulations of the urban circulation in the Salt Lake City area for CO₂ mod-
25 eling, *J. Appl. Meteorol. Clim.*, 52, 323–340, doi:10.1175/Jamc-D-12-061.1, 2013.
- Nordbo, A., Jarvi, L., Haapanala, S., Wood, C. R., and Vesala, T.: Fraction of natural area
as main predictor of net CO₂ emissions from cities, *Geophys. Res. Lett.*, 39, L20802,
doi:10.1029/2012gl053087, 2012.
- 30 Pataki, D. E., Alig, R. J., Fung, A. S., Golubiewski, N. E., Kennedy, C. A., McPherson, E. G.,
Nowak, D. J., Pouyat, R. V., and Lankao, P. R.: Urban ecosystems and the North American
carbon cycle, *Glob. Change Biol.*, 12, 2092–2102, doi:10.1111/J.1365-2486.2006.01242.X,
2006.

An attempt at estimating Paris area CO₂ emissions

F. M. Bréon et al.

Title Page

Abstract

Introduction

Conclusions

References

Tables

Figures

◀

▶

◀

▶

Back

Close

Full Screen / Esc

Printer-friendly Version

Interactive Discussion



- Pataki, D. E., Xu, T., Luo, Y. Q., and Ehleringer, J. R.: Inferring biogenic and anthropogenic carbon dioxide sources across an urban to rural gradient, *Oecologia*, 152, 307–322, doi:10.1007/S00442-006-0656-0, 2007.
- 5 Peylin, P., Rayner, P. J., Bousquet, P., Carouge, C., Hourdin, F., Heinrich, P., Ciais, P., and AEROCARB contributors: Daily CO₂ flux estimates over Europe from continuous atmospheric measurements: 1, inverse methodology, *Atmos. Chem. Phys.*, 5, 3173–3186, doi:10.5194/acp-5-3173-2005, 2005.
- Prairie, Y. T. and Duarte, C. M.: Direct and indirect metabolic CO₂ release by humanity, *Biogeosciences*, 4, 215–217, doi:10.5194/bg-4-215-2007, 2007.
- 10 Tarantola, A.: Inverse problem theory and methods for model parameter estimation, XII, Society for Industrial and Applied Mathematics, Philadelphia, PA, 342 pp., 2005.
- Widory, D. and Javoy, M.: The carbon isotope composition of atmospheric CO₂ in Paris, *Earth Planet. Sc. Lett.*, 215, 289–298, doi:10.1016/S0012-821x(03)00397-2, 2003.
- 15 Zhao, C. L. and Tans, P. P.: Estimating uncertainty of the WMO mole fraction scale for carbon dioxide in air, *J. Geophys. Res.-Atmos.*, 111, D08s09, doi:10.1029/2005jd006003, 2006.

An attempt at estimating Paris area CO₂ emissions

F. M. Bréon et al.

Title Page

Abstract

Introduction

Conclusions

References

Tables

Figures

◀

▶

◀

▶

Back

Close

Full Screen / Esc

Printer-friendly Version

Interactive Discussion



Table 1. Information about the CO₂ measuring stations that are used in this paper.

Location	Acronym	Latitude [°]	Longituded [°]	Height a.g.l. [m]	Distance from Paris centre [km]
Eiffel Tower	EIF	48.8582	2.2946	300	4 (W)
Montgé-en-Goële	MON	49.0284	2.7489	9	35 (NE)
Gonesse	GON	48.9908	2.4446	4	16 (N)
Gif sur Yvette	GIF	48.7100	2.1475	7	23 (SW)
Trainou Forest	TRN	47.9647	2.1125	180	101 (S)

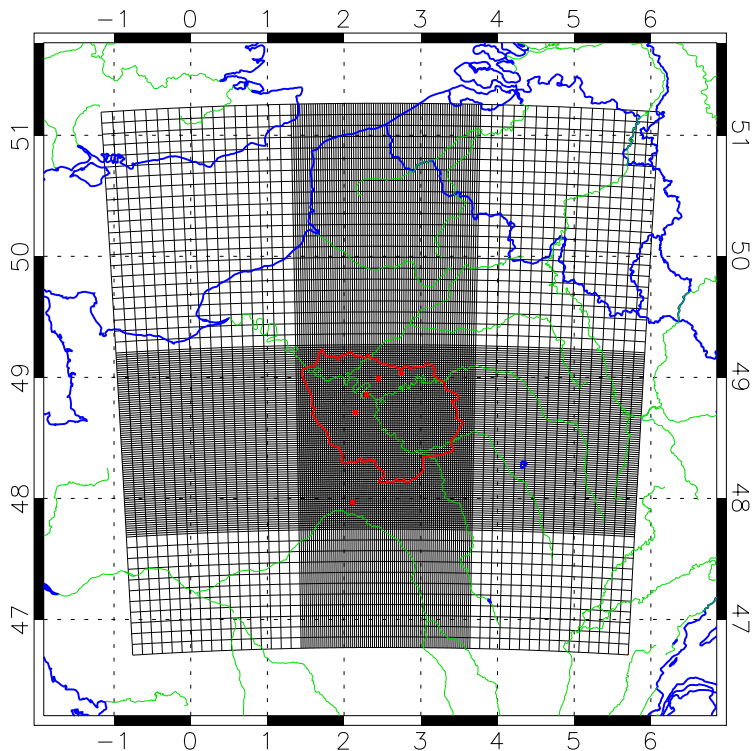


Fig. 1. Map of the study area showing the location of the continuous CO₂ measurement stations that are used in this paper (red dots). The black lines show the model grid with a 2 km resolution at the centre, and 10 km on the sides. The red line shows the limits of the Île-de-France region.

An attempt at
estimating Paris area
CO₂ emissions

F. M. Bréon et al.

Title Page

Abstract

Introduction

Conclusions

References

Tables

Figures

◀

▶

◀

▶

Back

Close

Full Screen / Esc

Printer-friendly Version

Interactive Discussion



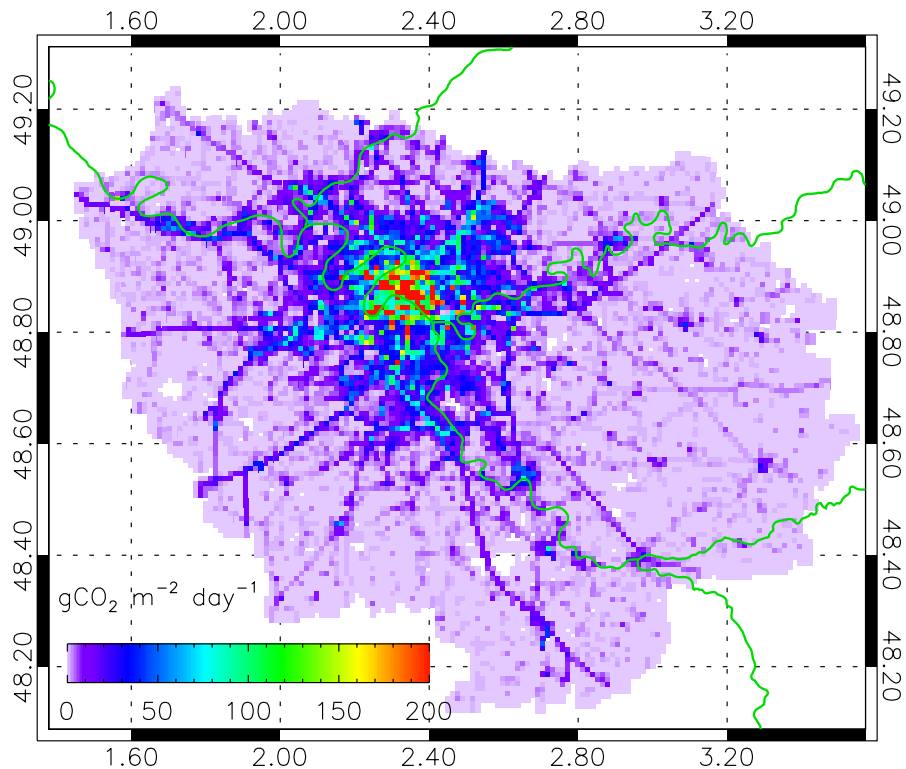


Fig. 2. Typical CO₂ emissions of Île-de-France, according to AirParif year 2008 inventory, for a weekday in October. The point sources are not included in this map. The emissions are provided for the area outlined in red in Fig. 1. The resolution is 1 km. The grid is 0.2° in latitude and 0.4° in longitude.

An attempt at estimating Paris area CO₂ emissions

F. M. Bréon et al.

Title Page

Abstract Introduction

Conclusions References

Tables Figures

◀ ▶

◀ ▶

Back Close

Full Screen / Esc

Printer-friendly Version

Interactive Discussion



An attempt at estimating Paris area CO₂ emissions

F. M. Bréon et al.

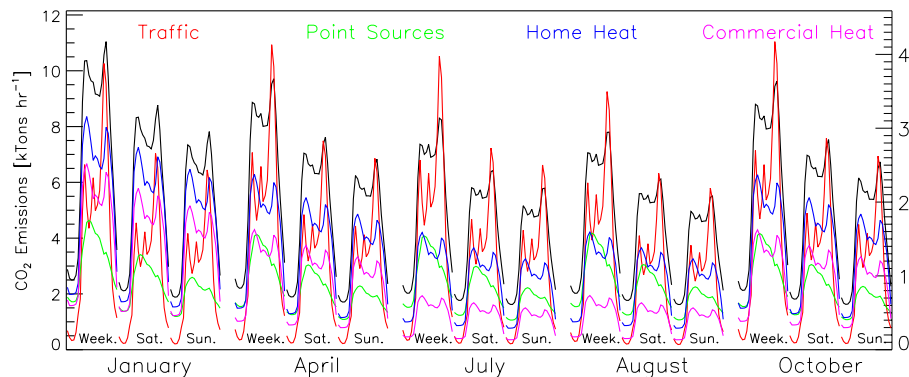


Fig. 3. Temporal variation of the main CO₂ emission sectors according to the AirParif inventory. The figure shows, for 5 typical months and 3 typical days (Weekday, Saturday, Sunday), the hourly CO₂ emissions. The black line is the total emission (left scale) while the four coloured lines are for different sectors (right scale).

[Title Page](#)[Abstract](#)[Introduction](#)[Conclusions](#)[References](#)[Tables](#)[Figures](#)[◀](#)[▶](#)[◀](#)[▶](#)[Back](#)[Close](#)[Full Screen / Esc](#)[Printer-friendly Version](#)[Interactive Discussion](#)

An attempt at estimating Paris area CO₂ emissions

F. M. Bréon et al.

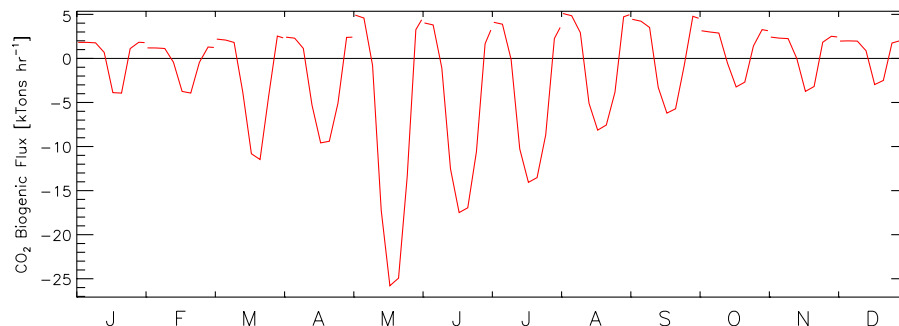


Fig. 4. Mean diurnal cycle of the biogenic flux (Net Ecosystem exchange) for the 12 calendar months and for the same area as in Figs. 2 and 3 which is outlined in red in Fig. 1. The values were derived from an average of the C-Tessel simulations.

[Title Page](#)[Abstract](#)[Introduction](#)[Conclusions](#)[References](#)[Tables](#)[Figures](#)[◀](#)[▶](#)[◀](#)[▶](#)[Back](#)[Close](#)[Full Screen / Esc](#)[Printer-friendly Version](#)[Interactive Discussion](#)

An attempt at estimating Paris area CO₂ emissions

F. M. Bréon et al.

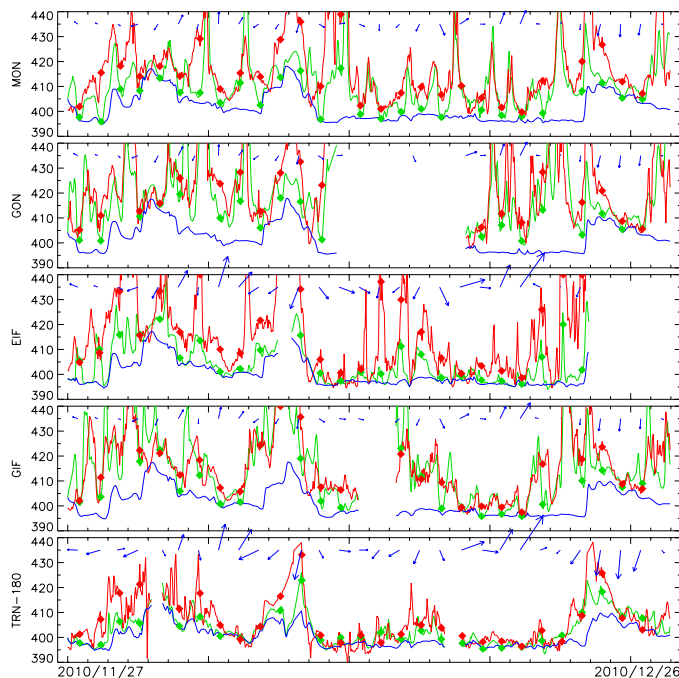


Fig. 5. Time series of the measured (red) and modelled (green) CO₂ mole fraction [ppm] for the five sites used in this paper (See Table 1). The symbols show the mean of the afternoon measurement/model values that are used for the inversion. The blue line is the background concentration modelled without the anthropogenic emissions or biogenic fluxes within the modelling domain. The blue arrows indicate the wind speed and direction at noon. A length equivalent to 1 day on the X-axis is for a wind speed of 10 m s⁻¹. This figure is for the 30 days period starting on 27 November 2010.

[Title Page](#)[Abstract](#)[Introduction](#)[Conclusions](#)[References](#)[Tables](#)[Figures](#)[◀](#)[▶](#)[◀](#)[▶](#)[Back](#)[Close](#)[Full Screen / Esc](#)[Printer-friendly Version](#)[Interactive Discussion](#)

An attempt at estimating Paris area CO₂ emissions

F. M. Bréon et al.

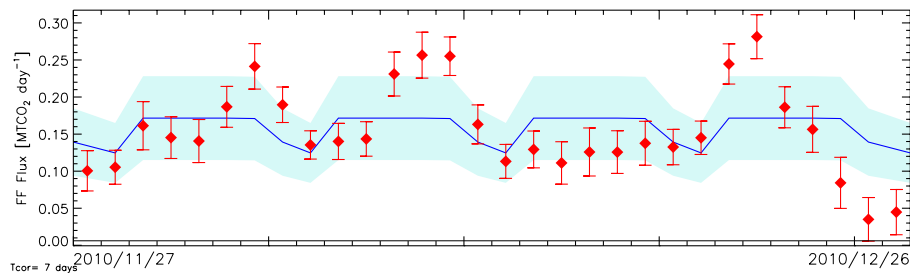


Fig. 6. Daily flux estimates of the anthropogenic emission for the 30 days of the period. The blue line shows the prior flux according to the AirParif inventory. Note the weekly cycle with lower values during Saturdays and Sundays. The red symbols and bars show the posterior estimates with their uncertainty range. This figure is for the November–December period. A similar figure for the October–November period is shown in the Appendix.

[Title Page](#)[Abstract](#)[Introduction](#)[Conclusions](#)[References](#)[Tables](#)[Figures](#)[◀](#)[▶](#)[◀](#)[▶](#)[Back](#)[Close](#)[Full Screen / Esc](#)[Printer-friendly Version](#)[Interactive Discussion](#)

An attempt at estimating Paris area CO₂ emissions

F. M. Bréon et al.

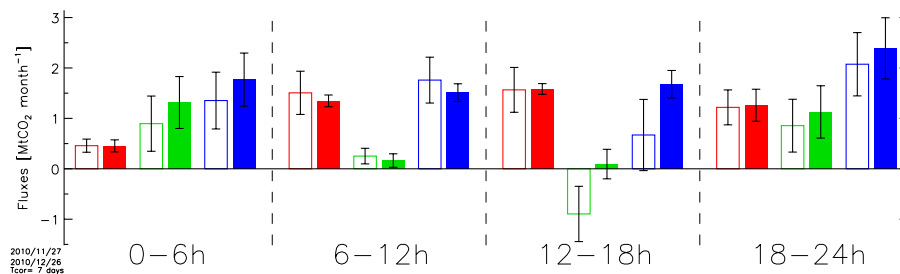


Fig. 7. Total flux estimates over the full 30 day period, for the 4 6 h periods. Red is for the anthropogenic emissions, green is for the biogenic fluxes while blue is for the total. The prior estimates are shown as open rectangles while the posterior are shown as filled rectangles. This figure is for the November–December period. A similar figure for the October–November period is shown in the Appendix.

[Title Page](#)[Abstract](#)[Introduction](#)[Conclusions](#)[References](#)[Tables](#)[Figures](#)[◀](#)[▶](#)[◀](#)[▶](#)[Back](#)[Close](#)[Full Screen / Esc](#)[Printer-friendly Version](#)[Interactive Discussion](#)

An attempt at estimating Paris area CO₂ emissions

F. M. Bréon et al.

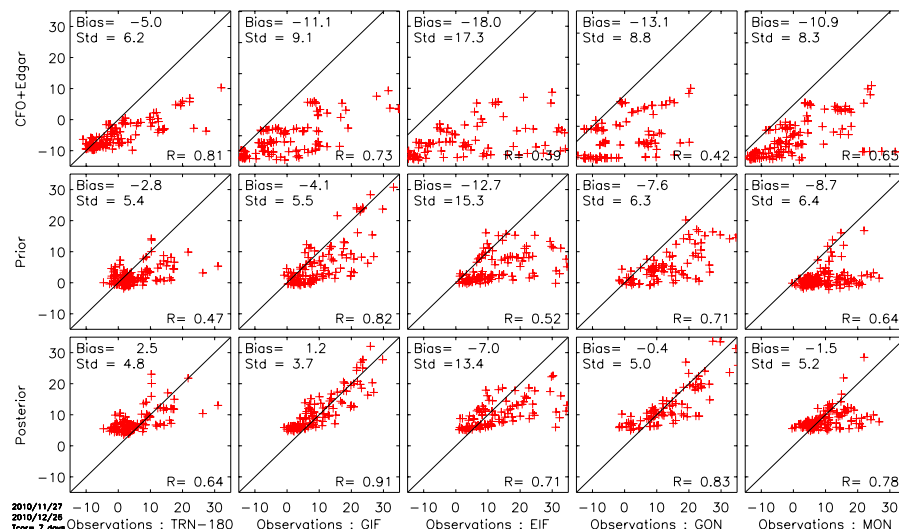


Fig. 8. Scatter plot of the measured and modelled concentration for the 5 stations used in this paper. The first line shows the mole fraction simulated using the boundary conditions and the anthropogenic emissions outside Île-de-France (y_F in Eq. 1) against the measurements. The values are offset by the mean of the measured concentrations. The second line shows the concentration estimates derived from the prior values for the biogenic fluxes and anthropogenic fluxes against the corrected measurements (i.e. $y - y_F$ in Eq. 1). The last line is the same but using the posterior estimates. This figure is for the November–December period. A similar figure for the October–November period is shown in the Appendix.

[Title Page](#)
[Abstract](#)
[Introduction](#)
[Conclusions](#)
[References](#)
[Tables](#)
[Figures](#)
[⏪](#)
[⏩](#)
[◀](#)
[▶](#)
[Back](#)
[Close](#)
[Full Screen / Esc](#)
[Printer-friendly Version](#)
[Interactive Discussion](#)


An attempt at estimating Paris area CO₂ emissions

F. M. Bréon et al.

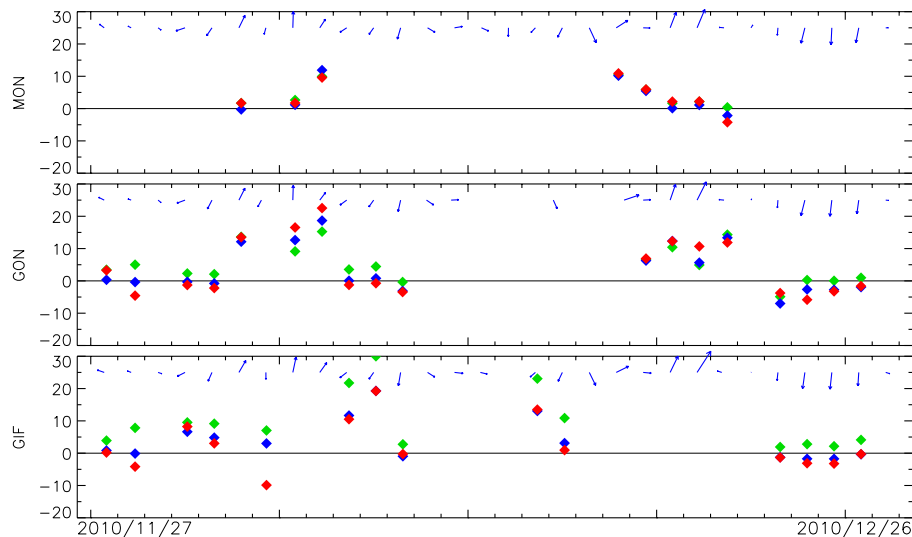


Fig. 9. Time series of the mole fraction differences between a station and another one used as a reference and selected based on the wind direction (see Sect. 3.3). The symbols show the mean afternoon concentrations (12 a.m.–4 p.m.) for the measurements (red), the prior (green) and the posterior (blue) estimates. As in Fig. 5, the arrows indicate the wind speed and direction. A similar figure for the other time period is shown in the Appendix.

[Title Page](#)[Abstract](#)[Introduction](#)[Conclusions](#)[References](#)[Tables](#)[Figures](#)[◀](#)[▶](#)[◀](#)[▶](#)[Back](#)[Close](#)[Full Screen / Esc](#)[Printer-friendly Version](#)[Interactive Discussion](#)

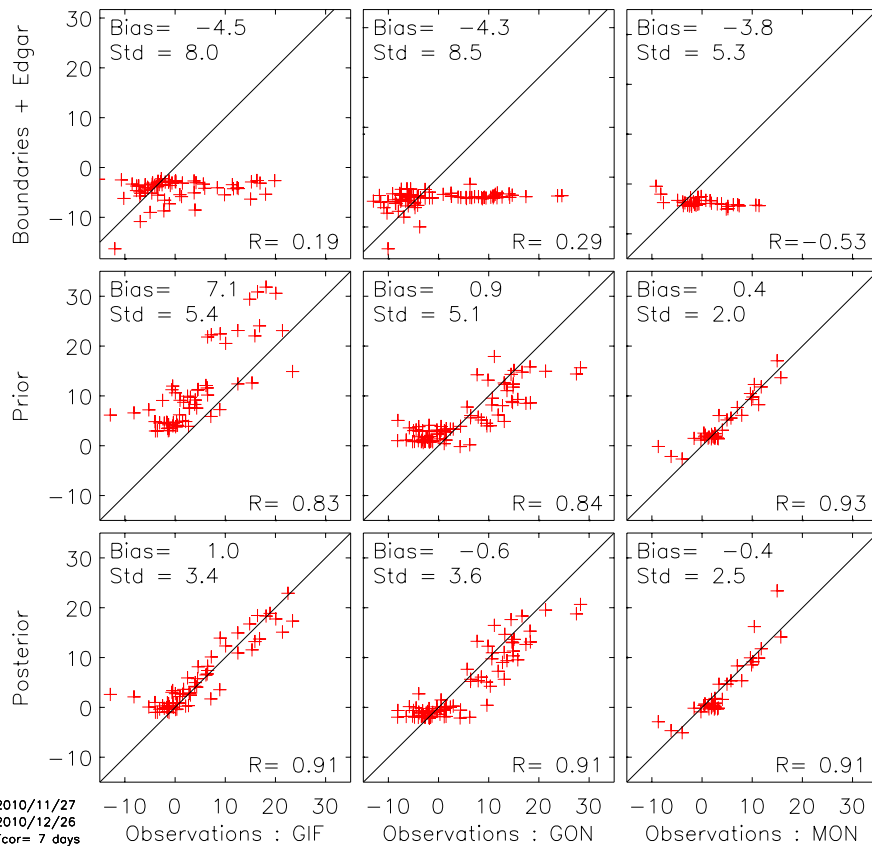


Fig. 10. Same as Fig. 8 but for the mole fraction gradients where the reference measurements is selected according to the wind direction. The TRN and EIF stations are not used. A similar figure for the other time period is shown in the Appendix.

An attempt at estimating Paris area CO₂ emissions

F. M. Bréon et al.

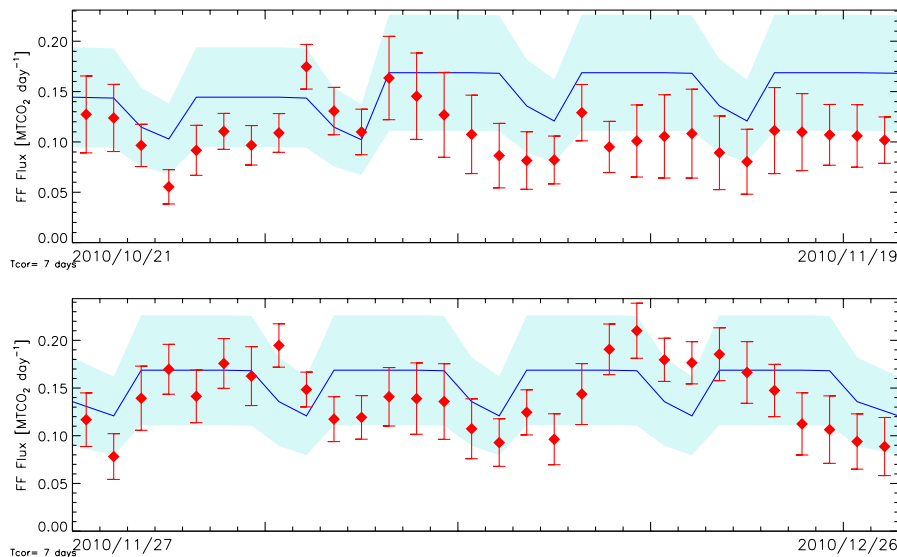


Fig. 11. Same as Fig. 6 but for the inversion based on the concentration gradients, and using only the three measuring stations in the vicinity of the Paris city. Both 30 day periods are shown.

[Title Page](#)[Abstract](#)[Introduction](#)[Conclusions](#)[References](#)[Tables](#)[Figures](#)[◀](#)[▶](#)[◀](#)[▶](#)[Back](#)[Close](#)[Full Screen / Esc](#)[Printer-friendly Version](#)[Interactive Discussion](#)

An attempt at estimating Paris area CO₂ emissions

F. M. Bréon et al.

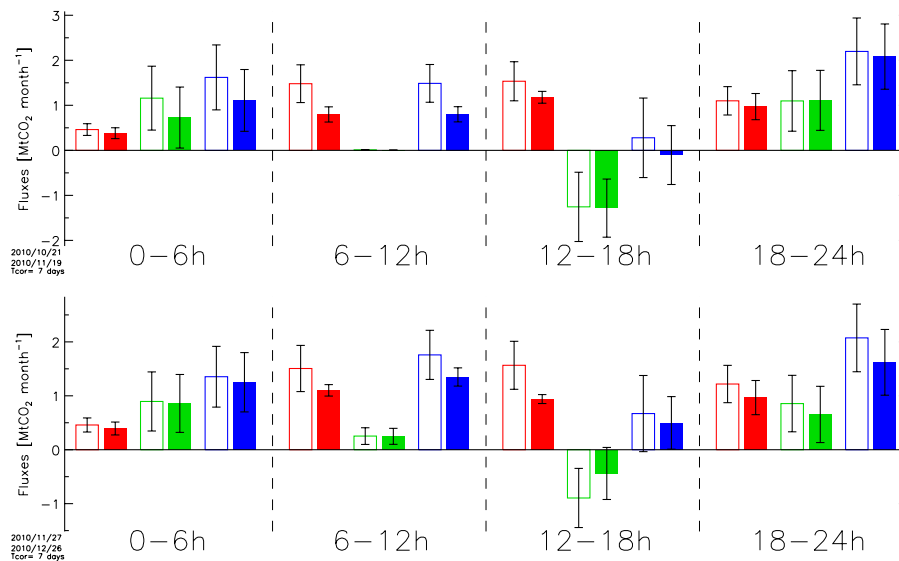


Fig. 12. Same as Fig. 7 but for the inversion based on the mole fraction gradients, and using only the three measuring stations in the vicinity of the Paris city. Both 30 day periods are shown.

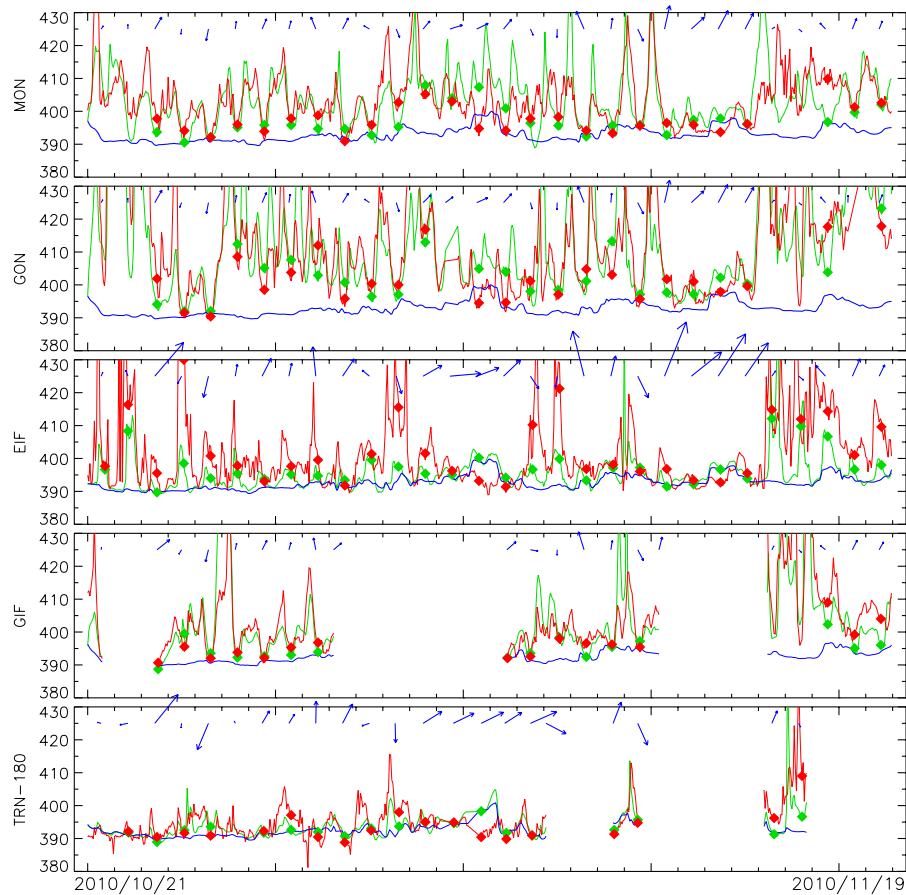


Fig. A1. Same as Fig. 5 but for the 30 day period starting on 21 October.

**An attempt at
estimating Paris area
CO₂ emissions**

F. M. Bréon et al.

Title Page	
Abstract	Introduction
Conclusions	References
Tables	Figures
◀	▶
◀	▶
Back	Close
Full Screen / Esc	
Printer-friendly Version	
Interactive Discussion	



An attempt at estimating Paris area CO₂ emissions

F. M. Bréon et al.

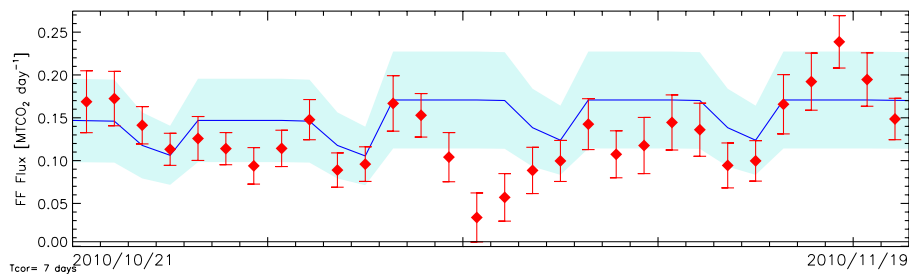


Fig. A2. Same as Fig. 6 but for the 30 day period starting on 21 October.

[Title Page](#)[Abstract](#)[Introduction](#)[Conclusions](#)[References](#)[Tables](#)[Figures](#)[◀](#)[▶](#)[◀](#)[▶](#)[Back](#)[Close](#)[Full Screen / Esc](#)[Printer-friendly Version](#)[Interactive Discussion](#)

An attempt at estimating Paris area CO₂ emissions

F. M. Bréon et al.

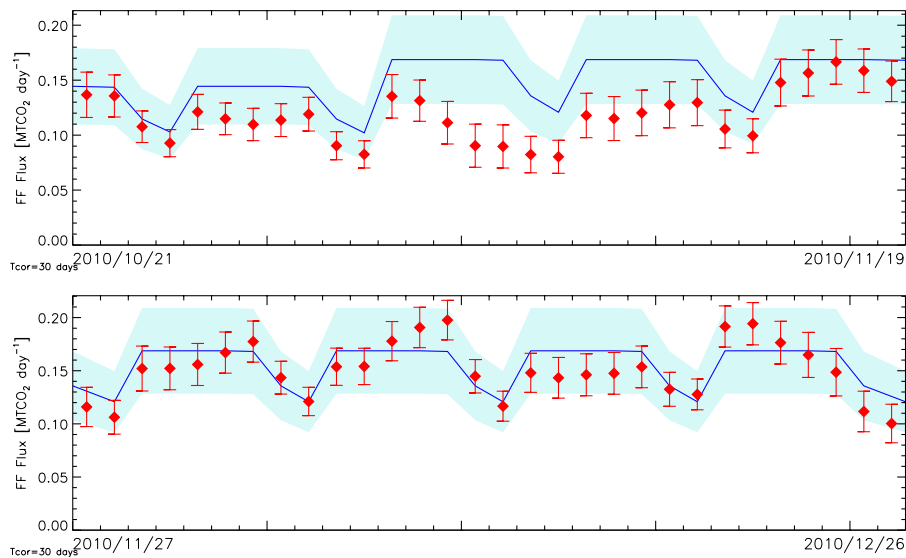


Fig. A3. Same as Fig. 6 but the covariance matrix **B** is build assuming a 30 day correlation time.

[Title Page](#)[Abstract](#)[Introduction](#)[Conclusions](#)[References](#)[Tables](#)[Figures](#)[◀](#)[▶](#)[◀](#)[▶](#)[Back](#)[Close](#)[Full Screen / Esc](#)[Printer-friendly Version](#)[Interactive Discussion](#)

An attempt at estimating Paris area CO₂ emissions

F. M. Bréon et al.

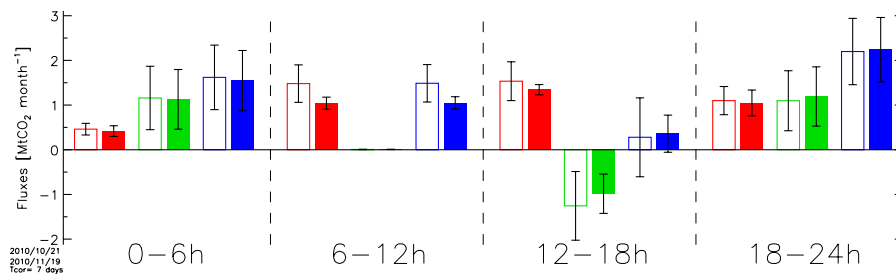


Fig. A4. Same as Fig. 7 but for the 30 day period starting on 21 October.

[Title Page](#)[Abstract](#)[Introduction](#)[Conclusions](#)[References](#)[Tables](#)[Figures](#)[⏪](#)[⏩](#)[◀](#)[▶](#)[Back](#)[Close](#)[Full Screen / Esc](#)[Printer-friendly Version](#)[Interactive Discussion](#)

An attempt at estimating Paris area CO₂ emissions

F. M. Bréon et al.

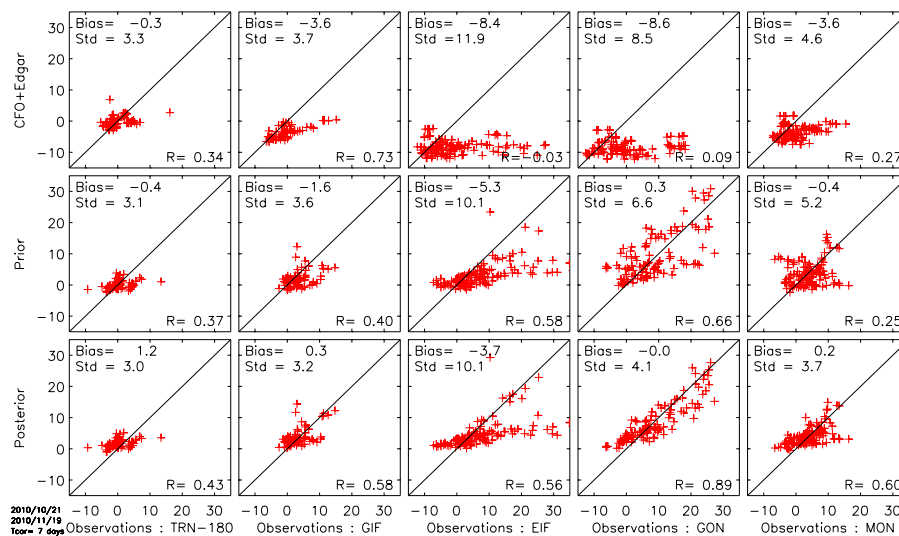


Fig. A5. Same as Fig. 8 but the 30 day period starting on 21 October.

Title Page

Abstract

Introduction

Conclusions

References

Tables

Figures

◀

▶

◀

▶

Back

Close

Full Screen / Esc

Printer-friendly Version

Interactive Discussion



An attempt at estimating Paris area CO₂ emissions

F. M. Bréon et al.

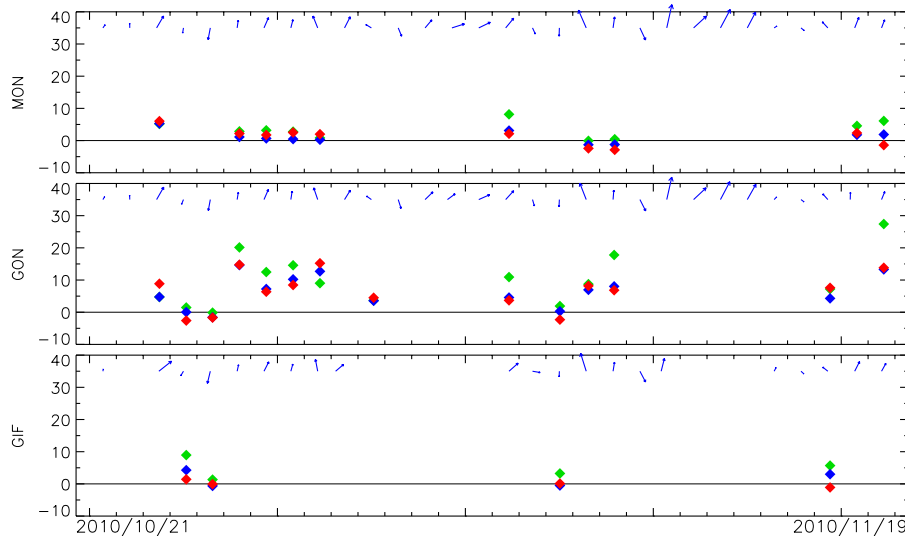


Fig. A6. Same as Fig. 9 but for the 30 day period starting on 21 October.

Title Page

Abstract

Introduction

Conclusions

References

Tables

Figures

◀

▶

◀

▶

Back

Close

Full Screen / Esc

Printer-friendly Version

Interactive Discussion



An attempt at estimating Paris area CO₂ emissions

F. M. Bréon et al.

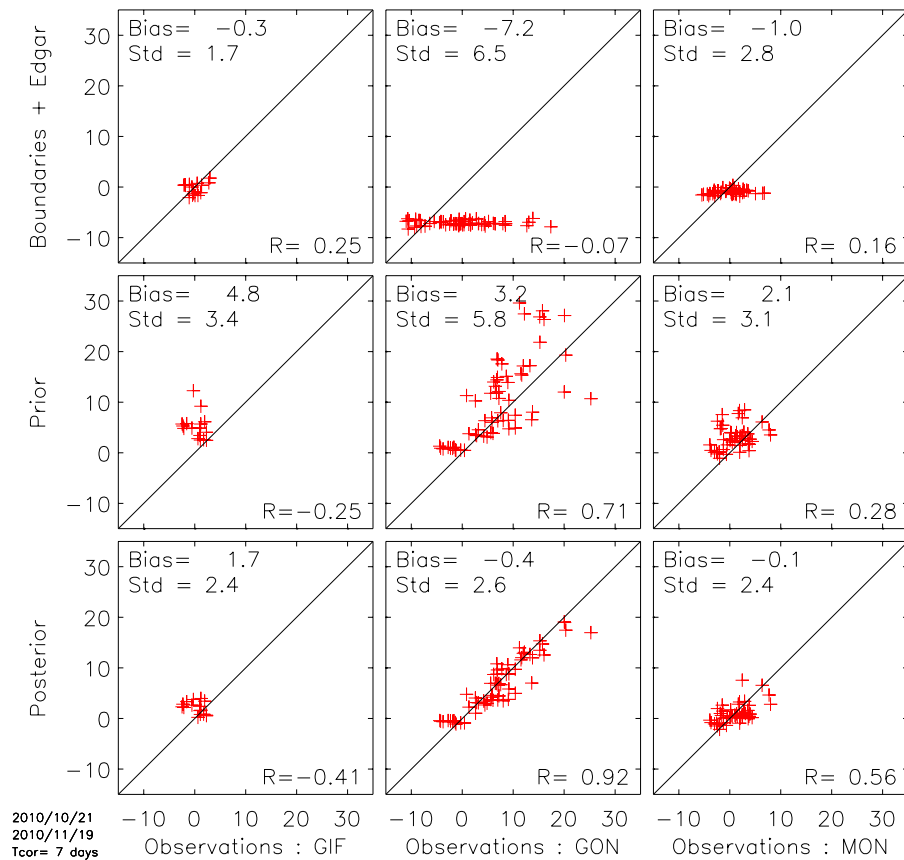


Fig. A7. Same as Fig. 10 but for the 30 day period starting on 21 October.

Title Page

Abstract Introduction

Conclusions References

Tables Figures

◀ ▶

◀ ▶

Back Close

Full Screen / Esc

Printer-friendly Version

Interactive Discussion

